

## REVIEW

View Article Online

View Journal | View Issue



Cite this: *Inorg. Chem. Front.*, 2020, **7**, 2890

# High pressure: a feasible tool for the synthesis of unprecedented inorganic compounds

Xuerong Wang and Xiaoyang Liu \*

Pressure can shorten the distance between molecules or atoms, which can change the periodicity of elements and provide more unprecedented novel materials. In order to produce substances that can remain stable or metastable under an atmospheric pressure, pressure has become an indispensable and powerful means. Recent research suggests that high-pressure synthesis methods have unlimited potential in different research fields. For example, high  $T_c$  (transition temperature) superconductors with a transition temperature of up to 250 K and super-hard nano-diamonds (NDs) with a hardness of 1 TPa can be synthesized under high-temperature and high-pressure (HTHP) conditions, and these materials cannot be achieved by other synthetic methods. Many recent research achievements involve the synthesis of some compounds with special structures and properties, such as high-entropy alloys, non-stoichiometric substances, inert element compounds, and heterostructure nanocrystals. This review will introduce the latest developments in inorganic compounds obtained under high pressure. Materials with different application backgrounds are classified, some materials with high performance or high potential are introduced, and possible synthesis mechanisms are discussed. In the Conclusions section, we summarize research directions in which the field of high-pressure synthesis research may have great breakthroughs in the next few years, and look forward to the future development of high-pressure synthesis methods.

Received 25th April 2020,  
Accepted 24th June 2020

DOI: 10.1039/d0qi00477d

rsc.li/frontiers-inorganic

## Introduction

After temperature and time, pressure has become the third condition and means of macroscopically affecting compound

State Key Laboratory of Inorganic Synthesis and Preparative Chemistry, College of Chemistry, Jilin University, Changchun 130012, Jilin, P. R. China.  
E-mail: liuxy@jlu.edu.cn



Xuerong Wang

Xuerong Wang was born in Huai'an, China, and received his bachelor's degree in chemistry from Changchun Normal University, in 2019. He is currently pursuing M.Sc. program at State Key Laboratory of Inorganic Synthesis & Preparative Chemistry, College of Chemistry, Jilin University under the guidance of Prof. Xiaoyang Liu. His research interests are the synthesis and phase transition of inorganic compounds under high temperature and high pressure conditions.



Xiaoyang Liu

Xiaoyang Liu was born in Dalian, China. From Jilin University of China, he obtained his B.Sc. degree (1987) in Inorganic Chemistry, and M.Sc. degree (1990) and Ph.D. (1993) in Condensed Matter Physics. From 1995 to 2004, as a post-doc or visiting scholar or research scientist, he worked at Osaka University (Japan), Regensburg University (Germany), University of California at Los Angeles (USA), and the University of Western Ontario (Canada), respectively. After that, he came back to China and joined the College of Chemistry, Jilin University. From 1987 to present, his main research interest has been inorganic synthesis under high pressure and high temperature conditions.



**Scheme 1** Schematic illustration of eight classification for the inorganic high pressure and high temperature synthesized materials. Reproduced with permission from ref. 2–9. Copyright 2016 to 2018, Wiley, AAAS, Elsevier, ACS and Nature.

synthesis, and plays a role in promoting the synthesis of materials. Under high-pressure conditions, new solid compounds that cannot be formed under conventional thermodynamic conditions can be formed, which makes the discovery of new compounds and new solid chemical bonds more interesting and complicated.<sup>1</sup> As shown in Scheme 1, compounds recently synthesized under high-temperature and high-pressure (HTHP) conditions can be classified into: (1) superconductors, (2) super-hard materials, (3) thermoelectric materials, (4) high energy density materials, (5) semiconductors, (6) nano-diamond and doped diamond, (7) non-stoichiometric compounds, and (8) some new phases and new materials synthesized by HPHT. Recent research suggests that iron-based compounds, hydrogen-rich compounds, and even organic compounds have the prospect of enhancing superconducting properties.<sup>10–12</sup> Iron-based superconductors can effectively resist impurities, and have been shown to have supercritical characteristics and excellent grain boundaries. Organic superconductors are regarded as a cleaner material, but hydrogen-rich hydrides are more competitive in the fields of hydrogen storage, high energy density, and metal hydrogen research.<sup>13</sup> Recent research on new super-hard materials suggests that it seems impossible to synthesize harder materials than diamond. In other words, the current exploration of super-hard materials should mainly target materials with a stronger performance than diamond applications, including hardness and stability under extreme working conditions.<sup>14,15</sup> The synthesis of thermoelectric materials is always challenging. Classic  $(\text{Bi}_{1-x}\text{Sb}_x)_2(\text{Se}_{1-y}\text{Te}_y)_3$  compound to  $\text{Ba}_8\text{Si}_{46}$  clathrate compound can demonstrate that the synthesis of new thermoelectric materials is still valuable.<sup>16</sup> The processes provide both extremely high pressure and high temperature for the synthesis of materials, and make some of the synthetic materials have the ability to store high-density

energy and release energy under appropriate conditions, which provides a wide range of applications for high energy density materials.<sup>17</sup> Research on the synthesis of azides under high pressure has obtained some preliminary results, but the exploration of high-energy density azides is still limited by the difficulties in preparation due to their high explosiveness and structural instability.<sup>18</sup> As a material synthesized under HPHT conditions, diamond has excellent hardness and remains stable when decompressed to ambient pressure, which makes diamond one of the most widely used materials. Although challenges such as lattice mismatch<sup>19</sup> and difficulty in synthesizing large single crystals<sup>20,21</sup> still exist, after further understanding of the carbon migration mechanism artificial diamond has gradually been widely used in semiconductor devices,<sup>22</sup> biochemical sensing,<sup>23</sup> electrocatalysis,<sup>24</sup> magnetic resonance imaging,<sup>25</sup> cancer treatment,<sup>26</sup> and other aspects. On the other hand, nano-scale diamond still has unparalleled performance, even better than ordinary diamond in some aspects, such as nano-diamond doping,<sup>27,28</sup> electrochemical coatings,<sup>29,30</sup> and even the establishment of biological neural connections.<sup>31,32</sup> Because of their excellent properties, nano-diamonds are still a hot topic in the fields of chemistry and materials research. Most of the materials mentioned above are obtained by high-pressure methods, but there have been no recent publications on better integration and induction of recent high-pressure research. This review aims to briefly introduce the important research achievements in the field of HPHT synthesis during the past five years. The purpose is to provide convenience to relevant researchers in order to more systematically understand the cutting-edge results of high-pressure synthesis obtained in recent years and use them to design and create new functional materials in a more systematic and effective way.

## Synthesis of unprecedented inorganic compounds

### Superconductor materials

Under the guidance of the Bardeen–Cooper–Schrieffer (BCS) theory, researchers have made attempts to make superconductors with higher transition temperatures. It is well known that electrons in heavily doped diamond can form a pair in the form of weak coupling at the temperature of liquid helium (4.2 K), commonly known as Cooper pairs, and exhibit superconductivity. The superconductivity of conventional superconductors arises from electron pairing mediated by the exchange of phonons, which result in a superfluid-like behavior. High pressure has had an important role in the discovery of conventional superconductors: of the 53 known element superconductors, 23 elements can become superconductive only at high pressure, while other elements still have potential high  $T_c$  superconductor compounds that can only appear under high pressure (Fig. 1).<sup>36</sup> Transmission electron microscopy (TEM) characterization of polycrystalline boron-doped superconducting diamond synthesized at 8–9 GPa confirmed the coexistence

**Fig. 1** Superconductive periodic table for elemental solids. The elements that are superconductive at ambient pressure are shaded in grey, the ones that are superconductive only at high pressure in blue. For both ambient-pressure and high-pressure elemental superconductors, the maximum superconducting critical temperature ( $T_c^M$ ) and the pressure needed to achieve it ( $P^*$ ) are indicated. Reproduced with permission from ref. 33–35. Copyright 2004, 2015 and 2002, IOP Publishing, Elsevier and Nature.

The concept of adjusting the composition mentioned in the BCS theory to maximize  $T_c$  has generated great interest in the research of metal and semimetal superconductors. For the semi-metal-filled skutterudite  $\text{CaOs}_4\text{P}_{12}$  with hole carriers, its resistivity, DC susceptibility and specific heat measurements show that its superconducting transition temperature  $T_c$  is less than 2.5 K. Regarding the thermoelectric coefficient, the measured value 1.4 is consistent with the BCS theoretically predicted value of 1.43, which means that  $\text{CaOs}_4\text{P}_{12}$  is thus classified as a BCS-type weakly-coupled type-II superconductor.<sup>41</sup> In addition to the hardness of conventional insulating hard materials, the covalent metal TaB's temperature-dependent resistivity measurement demonstrates that the metal's electrical conductivity is close to that of a conductor, and turns into a superconductor when  $T = 7.8$  K.<sup>42</sup>  $\text{Cu}_{11}\text{Bi}_7$ , another metastable material, was successfully synthesized under a pressure of 6 GPa and at a temperature of 800 K, and

Hydrogen-rich compounds can exhibit the characteristics of metal hydrogen atoms at higher pressures, but at pressures lower and more accessible than needed for metal hydrogen. Recent theoretical studies have predicted the high-pressure stability of hydrogen-rich compounds (see Table 1). According to model prediction results, under the conditions of a pressure above 40 GPa and a temperature of 2000 K,  $\text{NaH}_3$  and  $\text{NaH}_7$  sodium hydrides were successfully synthesized for the first time,<sup>57</sup> and  $\text{UH}_5$ ,  $\text{UH}_7$  and  $\text{UH}_8$  were synthesized under the pressure of 5 GPa, 31 GPa and 45 GPa respectively for the first time.<sup>58</sup> The phase of the lanthanum super-hydride  $\text{LaH}_{10}$  with a fcc lattice was synthesized at a pressure of 170 GPa established by La and  $\text{H}_2$  and heating to about 1000 K. The critical temperature of the synthesized  $\text{LaH}_{10}$  with the  $Fm\bar{3}m$  structure was found at about 250 K.<sup>2,59</sup> The  $\text{LaH}_{10}$  material achieved a superconductivity record near room temperature due to the



**Table 1** Calculated max  $T_c$ , stable pressure and space group of superconducting hydrides from the research of the past five years

| Hydride                        | Calculated max $T_c$ , K (pressure, GPa) | Space group | Ref. |
|--------------------------------|--|-------------|------|
| PrH <sub>9</sub>               | 9 (120)                                  | $P6_3/mmc$  | 65   |
| FeH <sub>6</sub>               | 46 (300)                                 | $C2/c$      | 43   |
| FeH <sub>5</sub>               | 51 (130)                                 | $I4/mmm$    | 44   |
| SnH <sub>4</sub>               | 62 (200)                                 | $P6_3/mmc$  | 45   |
| UH <sub>7</sub>                | 66 (0)                                   | $P6_3/mmc$  | 58   |
| MgGeH <sub>6</sub>             | 67 (200)                                 | $Pm3$       | 46   |
| CeH <sub>9</sub>               | 117 (200)                                | $P6_3/mmc$  | 63   |
| ScH <sub>6</sub>               | 130 (200)                                | $P6_3/mmc$  | 47   |
| MgH <sub>6</sub>               | 190 (200)                                | $Im3m$      | 48   |
| UH <sub>8</sub>                | 193 (0)                                  | $Fm3m$      | 58   |
| ThH <sub>10</sub>              | 221 (100)                                | $Fm3m$      | 49   |
| YH <sub>6</sub>                | 227 (237)                                | $Im3m$      | 50   |
| CaH <sub>6</sub>               | 235 (150)                                | $Im3m$      | 51   |
| AcH <sub>16</sub>              | 241 (150)                                | $P6m2$      | 52   |
| YH <sub>9</sub>                | 243 (201)                                | $P6_3/mmc$  | 50   |
| LaH <sub>10</sub> <sup>a</sup> | 250 (170)                                | $Fm3m$      | 59   |
| AcH <sub>10</sub>              | 251 (200)                                | $R3m$       | 52   |
| YH <sub>10</sub>               | 326 (300)                                | fcc         | 50   |

<sup>a</sup> Structure has been confirmed experimentally.

favorable Meissner effect (Fig. 2). It should be noted that this critical temperature is the highest critical temperature confirmed to date in superconducting materials. Potential superconducting metal compounds similar to LaH<sub>10</sub>, such as FeH<sub>5</sub> and CeH<sub>9</sub>, have become the best candidates for new high-temperature superconducting materials.<sup>60,61</sup> Considering that when synthesizing new materials under HPHT conditions, the

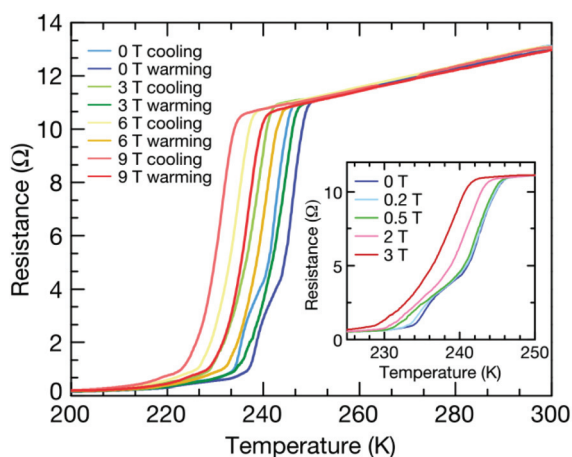


**Fig. 2** Meissner effect of LaH<sub>10</sub> under an external magnetic field. Electrical resistance as a function of temperature for LaH<sub>10</sub> (sample 3) under applied magnetic fields of up to 9 T. The width of the superconducting transition remains essentially constant up to 9 T. Both the cooling and heating temperature sweeps are plotted. The superconducting critical temperatures were determined as the average of the two sweeps. An applied field of 9 T reduces the onset of the superconducting transition from around 250 K (as extracted from the heating curve) to around 240 K. It is notable that the step observed in the superconducting transition measured at zero field, which appears around 245 K, disappears under the application of a modest field of just 3 T (inset). Reproduced with permission from ref. 59. Copyright 2019, Nature.

phase transition of the material will change the relationship between the hydrogen content and the critical temperature of the material to a certain extent, which can help us improve the  $T_c$  of the material.<sup>62</sup> Due to the need for extremely high pressure to stabilize the presence of hydrogen-rich hydride, this greatly limits the application of materials such as FeH<sub>5</sub> (stabilized pressure 130 GPa) and LaH<sub>10</sub> (stabilized pressure 170 GPa). Therefore, reducing the pressure at which hydrogen-rich hydrides exist stably has become another research challenge. The synthesis of cerium hydride in diamond anvil cells (DAC) (synthesis pressure 80–100 GPa) provides some guidance for reducing the synthesis pressure, because the use of laser heating can reduce the pressure required to maintain the stable existence of hydrogen-rich hydride to some extent.<sup>63</sup> Peng *et al.* first studied all candidate structures of rare earth superhydrides with H-rich cages under high pressure, and proposed that only several hydrides could be superconductors with  $T_c > 77$  K.<sup>64</sup> Continuing studies of lanthanide superhydrides to explain the mechanism and the synchrotron X-ray diffraction analysis at 120 GPa demonstrated the presence of previously predicted  $F43m$ -PrH<sub>9</sub> and unexpected  $P6_3/mmc$ -PrH<sub>9</sub> phases. Another run of experiments confirmed the existence of the pronounced superconducting resistance drop in PrH<sub>9</sub> below 9 K.<sup>65</sup> Due to the coexistence of magnetic order and likely superconductivity in a very close range of pressures of praseodymium hydrides, this allows us to infer that magnetic properties may have an effect on the low superconducting transition temperature  $T_c$  and to elucidate the great influence of metal atoms on the superconductivity of superhydrides.

### Super-hard materials

Researchers have focused on novel super-hard materials for several decades based on both practical and scientific purposes. To make a material super-hard, its structure must consist of a closely packed network of 3D strong covalent bonds. Pressure has become an important technique for synthesizing super-hard materials, because it induces volume decreases that stabilize densely packed structures. Compounds such as Mn<sub>3</sub>B<sub>4</sub>, δ-WN, MoSi<sub>2</sub>, and VB<sub>2</sub> are composed of light elements (B, C, and N) and heavy transition elements, which may result in a high valence electron density in the compounds (see Table 2). The high-valence electron density can

**Table 2** Sintering pressure, temperature and Vickers hardness of super-hard compounds fabricated using the references mentioned in this article

| Samples                          | Sintering pressure (GPa) | Sintering temperature (K) | Vickers hardness (GPa) | Ref. |
|----------------------------------|--------------------------|---------------------------|------------------------|------|
| Mn <sub>3</sub> B <sub>4</sub>   | 5                        | 1750                      | 16.3                   | 66   |
| δ-WN                             | 5.2                      | 2073                      | 13.8                   | 67   |
| WB <sub>2</sub>                  | 5.2                      | 1873                      | 25.5                   | 71   |
| MoSi <sub>2</sub>                | 5.5                      | 1573                      | 15                     | 68   |
| β-Si <sub>3</sub> N <sub>4</sub> | 5.5                      | 2173                      | 19.9 ± 0.6             | 70   |
| VB <sub>2</sub>                  | 8                        | 1700                      | 27.2 ± 1.5             | 69   |

realize the resistance to elastic and plastic deformation, and the double zig-zag boron chains in the  $\text{Mn}_3\text{B}_4$  structure form a strong covalent skeleton. Therefore, the integrity of the structure is strengthened, giving it a high hardness, which in turn provides us with a new structure for the design of universal high-hardness materials.<sup>66</sup> In the process of synthesizing  $\delta\text{-WN}$ ,  $\text{W}_2\text{N}_3$  and melamine were used as tungsten and nitrogen sources, respectively. Electron localization function (ELF), density of states (DOS) and Mulliken population analysis methods were used to explore the bonding methods in  $\delta\text{-WN}$ , and it was found that the hardness of  $\delta\text{-WN}$  did not meet the expectations due to the lack of strong W-N covalent bonds to form a three-dimensional network structure.<sup>67</sup> Sintered  $\text{MoSi}_2$  has excellent physical properties, including a high relative density ( $6.23 \text{ g cm}^{-3}$ ), Vickers hardness (15.0 GPa), and fracture toughness ( $10.7 \text{ MPa m}^{-1/2}$ ) when pressure is applied.<sup>68</sup>  $\text{VB}_2$  has the characteristics of high hardness ( $27.2 \pm 1.5 \text{ GPa}$ ), refractory ceramic (stable at 1410 K in air) and excellent electrical conductivity ( $41 \mu\Omega \text{ cm}^{-1}$ ).<sup>69</sup> The reduced grain size contributed to the improved hardness and fracture toughness. The measured Vickers hardness  $H_V$  of the submicron-sized polycrystalline  $\beta\text{-Si}_3\text{N}_4$  could reach up to about 20 GPa, approaching the upper limit of single crystal  $\beta\text{-Si}_3\text{N}_4$ .<sup>70</sup> The maximum asymptotic Vickers hardness is 25.5 GPa for  $\text{WB}_2$  with a grain size of 300 nm which is a 10% increase compared to  $\text{WB}_2$  with a grain size of 3  $\mu\text{m}$ . The Vickers indentation test

showed that the Vickers hardness of  $\text{WB}_2$  decreased as the grain size grew larger.<sup>71</sup>

### Thermoelectric compounds

Thermoelectric materials are a kind of functional semiconductor material that use solid internal carrier movement to realize the conversion of thermal energy and electrical energy. They have the characteristics of high stability, flexible size, and no pollution. Therefore, making these materials into a functional device and working in special environments have potential valuable applications. A heavily doped semiconductor has been recognized as a good thermoelectric material, and the  $(\text{Bi}_{1-x}\text{Sb}_x)_2(\text{Se}_{1-y}\text{Te}_y)_3$  alloy family has become the best commercial thermoelectric material in recent years.

HPHT conditions have a significant effect on the synthesis of new clathrate compounds. Under HPHT conditions, the clathrate compound can be effectively doped and eventually form a heavily doped thermoelectric material with uniform composition. Compared to other preparation methods, the HPHT method has some unique advantages in the synthesis, and the thermoelectric performance of the bulk materials, including the ability to tune rapidly and cleanly, thus restrains the disorder phase separation during the preparation of materials. Current thermoelectric materials are roughly classified into several materials such as  $\text{Bi}_2\text{Te}_3$ ,  $\text{Sb}_2\text{Te}_3$ ,  $\text{PbTe}$ ,  $\text{SiGe}$ ,  $\text{CoSb}_3$  (skutterudite),  $\text{Zn}_4\text{Sb}_3$ ,  $\text{Ba}_8\text{Si}_{46}$  (metal silicide),  $\text{NaCo}_2\text{O}_4$  (transition metal oxide) *etc.* Table 3

**Table 3** Sample, sintering pressure, sintering temperature,  $ZT_{\text{max}}$ ,  $ZT_{\text{max}}$  sample composition,  $ZT_{\text{max}}$  temperature and source of thermoelectric materials fabricated using the references mentioned in this article

| Sample   | Sintering pressure (GPa) | Sintering temperature (K) | $ZT_{\text{max}}$ | $ZT_{\text{max}}$ sample composition (pressure, GPa)                                 | $ZT_{\text{max}}$ temperature (K) | Ref. |
|--|--------------------------|---------------------------|-------------------|--|-----------------------------------|------|
| $\text{Ba}_{8-x}\text{Eu}_x\text{Cu}_6\text{Si}_{40}$                    | 3                        | 1110                      | 0.16              | $\text{Ba}_8\text{Cu}_6\text{Si}_{40}$   | 720                               | 77   |
| $\text{Ba}_8\text{Cu}_x\text{Ge}_y\text{Si}_{46-x-y}$                    | 3.5                      | 1100                      | 0.25              | $\text{Ba}_8\text{Cu}_6\text{Ge}_{20}\text{Si}_{20}$                                 | 720                               | 74   |
| $\text{Bi}_2\text{Se}_3$   | 1–4                      | 1073                      | 0.37              | $\text{Bi}_2\text{Se}_3$ (1)   | 560                               | 80   |
| $\text{Ba}_8\text{Cu}_6\text{Ge}_{8x}\text{Si}_{40-8x}$                  | 3                        | 1125                      | 0.42              | $\text{Mn}_2\text{ScSbO}_6$  | 673                               | 76   |
| $\text{PbSe}_{1-x}\text{S}_x$  | 2                        | 903                       | 0.46              | $\text{PbSe}_{0.88}\text{S}_{0.12}$  | 573                               | 85   |
| $\text{Ba}_8\text{Ga}_{16}\text{In}_x\text{Ge}_{30-x}$                   | 3                        | 1083                      | 0.52              | $\text{Ba}_8\text{Ga}_{16}\text{In}_{1.5}\text{Ge}_{28.5}$                           | 773                               | 78   |
| $\text{Ba}_8\text{Cu}_6\text{Si}_{16}\text{Ge}_{24}$                     | 3–5                      | 1125                      | 0.55              | $\text{Ba}_8\text{Cu}_6\text{Si}_{16}\text{Ge}_{24}$ (4)                             | 673                               | 75   |
| $\text{Ba}_{0.2}\text{Co}_4\text{Sb}_{11.5}\text{Te}_{0.5}$              | 1.5–3.5                  | 900                       | 0.61              | $\text{Ba}_{0.2}\text{Co}_4\text{Sb}_{11.5}\text{Te}_{0.5}$ (3)                      | 723                               | 92   |
| $\text{Mg}_{2.02-x}\text{Al}_x\text{Si}_{1-3y}\text{Bi}_{2y}\text{Sb}_y$ | 3.5                      | 1073                      | 0.9               | $\text{Mg}_{1.96}\text{Al}_{0.06}\text{Si}_{0.985}\text{Bi}_{0.01}\text{Sb}_{0.005}$ | 773                               | 100  |
| $\text{In}_{0.3}\text{Co}_4\text{Sb}_{11.5}\text{Te}_{0.5}$              | 1–3                      | 900                       | 0.93              | $\text{In}_{0.3}\text{Co}_4\text{Sb}_{11.5}\text{Te}_{0.5}$ (3)                      | 711                               | 93   |
| $\text{Pb}_x\text{Co}_4\text{Sb}_{11.5}\text{Te}_{0.5}$                  | 1.5–3.5                  | 900                       | 0.93              | $\text{Pb}_{0.2}\text{Co}_4\text{Sb}_{11.5}\text{Te}_{0.5}$ (3.5)                    | 773                               | 94   |
| $\text{Mg}_2\text{Si}_{1-x}\text{Sb}_x$                                  | 3                        | 973                       | 0.94              | $\text{Mg}_2\text{Si}_{0.985}\text{Sb}_{0.015}$                                      | 873                               | 99   |
| $\text{Bi}_{0.5}\text{Sb}_{1.5}\text{Te}_{3-x}\text{Se}_x$               | 2.4                      | 900                       | 0.95              | $\text{Bi}_{0.5}\text{Sb}_{1.5}\text{Te}_{2.7}\text{Se}_{0.3}$                       | 503                               | 82   |
| $\text{In}_x\text{Ba}_y\text{Co}_4\text{Sb}_{12}$                        | 1                        | 900                       | 0.97              | $\text{In}_{0.4}\text{Ba}_{0.1}\text{Co}_4\text{Sb}_{12}$                            | 723                               | 89   |
| $\text{Mg}_2\text{Si}_{1-x}\text{Bi}_x$                                  | 2                        | 973                       | 0.98              | $\text{Mg}_2\text{Si}_{0.985}\text{Bi}_{0.015}$                                      | 883                               | 98   |
| $\text{Co}_4\text{Sb}_{12-x}\text{Te}_x$                                 | 2.3                      | 900                       | 1.03              | $\text{Co}_4\text{Sb}_{11.5}\text{Te}_{0.5}$   | 710                               | 91   |
| $\text{Yb}_x\text{Ba}_{8-x}\text{Ga}_{16}\text{Ge}_{30}$                 | 5                        | 1103                      | 1.1               | $\text{Yb}_{0.5}\text{Ba}_{7.5}\text{Ga}_{16}\text{Ge}_{30}$                         | 950                               | 79   |
| $\text{In}_x\text{Ba}_{0.2-x}\text{Co}_4\text{Sb}_{11.5}\text{Te}_{0.5}$ | —                        | 900                       | 1.11              | $\text{In}_{0.15}\text{Ba}_{0.05}\text{Co}_4\text{Sb}_{11.5}\text{Te}_{0.5}$         | 765                               | 90   |
| $\text{CoSb}_{2.75}\text{Te}_{0.20}\text{Sn}_{0.05}$                     | 1–3                      | 973                       | 1.17              | $\text{CoSb}_{2.75}\text{Te}_{0.20}\text{Sn}_{0.05}$ (3)                             | 793                               | 97   |
| $\text{In}_{0.15}\text{Ba}_{0.35}\text{Co}_4\text{Sb}_{12}$              | 2.5–3.5                  | 900                       | 1.18              | $\text{In}_{0.15}\text{Ba}_{0.35}\text{Co}_4\text{Sb}_{12}$ (3)                      | 723                               | 87   |
| $\text{Cu}_x\text{Bi}_{0.5}\text{Sb}_{1.5-x}\text{Te}_3$                 | 2                        | 890                       | 1.2               | $\text{Cu}_{0.005}\text{Bi}_{0.5}\text{Sb}_{1.495}\text{Te}_3$                       | 473                               | 81   |
| Graphene/BiSbTe  | 4                        | 625                       | 1.26              | $\text{Bi}_{0.4}\text{Sb}_{1.6}\text{Te}_3$ with 0.05 wt% graphene                   | 423                               | 84   |
| CNTs/BiSbTe  | 4                        | 930                       | 1.42              | $\text{Bi}_{0.4}\text{Sb}_{1.6}\text{Te}_3$ with 0.1 wt% CNTs                        | 373                               | 83   |
| $\text{Co}_4\text{Sb}_{11.7-x}\text{Te}_x\text{Sn}_{0.3}$                | 0.5–3                    | 1000                      | —                 | —  | —                                 | 95   |
| $\text{Ba}_x\text{In}_{0.2-x}\text{Co}_4\text{Sb}_{11.5}\text{Te}_{0.5}$ | 1–3                      | 900                       | —                 | —  | —                                 | 88   |
| $\text{Co}_4\text{Sb}_{11-x-y}\text{Te}_x\text{Sn}_y\text{Se}_y$         | 1–3                      | 900                       | —                 | —  | —                                 | 96   |
| $\text{In}_{0.5}\text{Sn}_x\text{Co}_4\text{Sb}_{12}$                    | 2.8–3.8                  | 321–710                   | —                 | —  | —                                 | 86   |
| $\text{Ba}_8\text{Al}_x\text{Si}_{46-x}$                                 | 3                        | 700                       | —                 | —  | —                                 | 73   |
| $\text{In}_x\text{Co}_4\text{Sb}_{12}$                                   | 7.5                      | 1243                      | —                 | —  | —                                 | 4    |

shows specific information of thermoelectric materials that have been researched and progressed in the direction of HPHT synthesis in the past five years.<sup>72</sup> X-ray diffraction analysis and structural reconstruction indicated that Al-doped  $\text{Ba}_8\text{Al}_x\text{Si}_{46-x}$  based on  $\text{Ba}_8\text{Si}_{46}$  is a type-I cage structure with a space group of  $Pm\bar{3}n$ . The doping of Al will increase the Seebeck coefficient (thermoelectric heating of semiconductor materials) and power factor, and they will show an increasing trend with increasing temperature.<sup>73</sup> For the clathrate compound  $\text{Ba}_8\text{Cu}_x\text{Ge}_y\text{Si}_{46-x-y}$ , with the increase of Cu and Ge content, the lattice defects will increase, its thermal conductivity will be significantly reduced, and the maximum  $ZT$  value (thermoelectric figure of merit) of  $\text{Ba}_8\text{Cu}_6\text{Ge}_{24}\text{Si}_{16}$  is 0.55 at a temperature of 673 K and a pressure of 4 GPa.<sup>74–76</sup> In the Eu and Cu-doped clathrate  $\text{Ba}_{8-x}\text{Eu}_x\text{Cu}_6\text{Si}_{40}$ , the substitution of Eu reduces the nano-morphology defects of the sample, and its Seebeck coefficient and power factor are reduced, thereby increasing its thermal conductivity. For  $\text{Ba}_8\text{Cu}_6\text{Si}_{40}$ , a minimum thermal conductivity of  $1.26 \text{ W m}^{-1} \text{ K}^{-1}$  was obtained at 720 K.<sup>77</sup> After doping, the type I clathrates  $\text{Ba}_8\text{Si}_{46}$  and  $\text{Ba}_8\text{Ga}_{16}\text{Ge}_{30}$  have their thermoelectric properties significantly improved. After doping with In,  $\text{Ba}_8\text{Ga}_{16}\text{In}_x\text{Ge}_{30-x}$  (Fig. 3) showed a decrease in Seebeck coefficient and resistivity, and the measured thermal conductivity was  $0.84 \text{ W m}^{-1} \text{ K}^{-1}$  and the  $ZT$  value was 0.52.<sup>78</sup> Recently, it has been successfully demonstrated that the Ge-based clathrate compound  $\text{Yb}_{0.5}\text{Ba}_{7.5}\text{Ga}_{16}\text{Ge}_{30}$  synthesized under a pressure of 5 GPa and a temperature of 773 K has a higher  $ZT$  value of 1.13.<sup>79</sup> These results show that, compared with other materials, type I clathrates still have complex and diverse situations in terms of improving the thermoelectric performance.

For  $\text{Bi}_2\text{Te}_3$ -based materials, the most recent research shows that  $\text{T-Bi}_2\text{Se}_3$  consolidated by spark plasma sintering (SPS) exhibits an anisotropic structure.<sup>80</sup> A small amount of Cu doping can enhance the thermoelectric performance of polycrystalline  $\text{Cu}_x\text{Bi}_{0.5}\text{Sb}_{1.5-x}\text{Te}_3$ , and successfully achieve a  $ZT$  value of 1.20 at 473 K.<sup>81</sup> Due to the influence of synthesis

pressure and Sb/Se co-doping, the quaternary  $\text{Bi}_{0.5}\text{Sb}_{1.5}\text{Te}_{3-x}\text{Se}_x$  alloy has formed abundant lattice defects in the microstructure, which is considered to be the scattering center of phonons, thereby reducing the thermal conductivity. Among them, the samples synthesized with the optimal ratio at a temperature of 503 K obtained the maximum  $ZT$  value of 0.95.<sup>82</sup>

Carbon nanotubes (CNTs) intrinsically exhibit high carrier mobility and high electrical conductivity. At the same time, the dispersed CNTs in the thermoelectric matrix can enhance the phonon scattering at the interface. Due to the doping of CNTs, the CNT-composited  $\text{BiSbTe}$  nanostructure bulk material could distinctly decrease the thermal conductivity at the multiscale interface through full-spectrum-phonon scattering, and enhance the Seebeck coefficient of the material by the low energy carrier filtering effect. When the concentration of CNTs was 0.05 wt%, a maximum  $ZT$  value of 1.42 was obtained at 373 K and 4 GPa.<sup>83</sup> Similar to carbon nanotubes, graphene also possesses high in-plane carrier thermal conductivity. Additionally, the numerous hetero-interfaces between graphene and the  $\text{Bi}_2\text{Te}_3$  matrix can further hinder phonon transport. This result could explain why a high concentration of graphene will weaken doping effects and scatter carriers. In terms of results, the graphene-composited  $\text{Bi}_{0.4}\text{Sb}_{1.6}\text{Te}_3$  sample reached the maximum  $ZT$  value of 1.26 at 423 K when the content of graphene was as low as 0.05 wt%.<sup>84</sup> Introduction of high pressure into the synthesis stage could reduce the reactive activation energy and improve the synthesis efficiency. For example, compared with  $\text{PbSe}$ , all  $ZT$  values of solid solutions  $\text{PbSe}_{1-x}\text{S}_x$  kept rising during the whole measurement interval, which meant that the solid solution treatment could modulate the electrical conduction type and the figure of merit effectively. Finally, of all the synthesis samples,  $\text{PbSe}_{0.88}\text{S}_{0.12}$  achieved both the highest PF (power factor) and the lowest thermal conductivity.<sup>85</sup>

As a thermoelectric material in the middle temperature range, skutterudite is widely used to generate electricity. Because of the excellent doping ability in the voids of the skutterudite structure, the thermoelectric properties can be significantly improved by changing the doping composition. The greater the amount of In introduced into  $\text{CoSb}_3$ , the smaller the charge of indium atoms, which means that the increase in the In content in  $\text{InCo}_4\text{Sb}_{12}$  leads to a much higher carrier concentration compared to  $\text{In}_{0.4}\text{Co}_4\text{Sb}_{12}$ , while the absolute value of Seebeck efficiency is lower.<sup>4</sup> On this basis, researchers have tried different doping methods, such as the co-doping of In–Sn,<sup>86</sup> In–Ba,<sup>87</sup> In–Ba–Te<sup>88</sup> and so forth. What caught our attention is that all the measures we mentioned before showed very low thermal conductivity, and the maximum  $ZT$  value showed good performance. For example, the maximum  $ZT$  value of the  $\text{In}_{0.4}\text{Ba}_{0.1}\text{Co}_4\text{Sb}_{12}$  sample reached 0.97 at 723 K,<sup>89</sup> and the  $\text{In}_{0.15}\text{Ba}_{0.05}\text{Co}_4\text{Sb}_{11.5}\text{Te}_{0.5}$  sample showed a high  $ZT$  value of 1.11.<sup>90</sup>

Another way to improve the thermoelectric properties of  $\text{CoSb}_3$  materials is to dope them with Te. For the single-phase skutterudite compound  $\text{Co}_4\text{Sb}_{12-x}\text{Te}_x$ , the  $ZT$  value reaches a



**Fig. 3** The crystal structure of type-I  $\text{Ba}_8\text{Ga}_{16}\text{In}_x\text{Ge}_{30-x}$  clathrate contains 20- and 24-atom polyhedra. The small atoms represent the frame elements, the larger atoms are filled with atoms, and the different colors represent different atoms. Reproduced with permission from ref. 78. Copyright 2018, Elsevier.

maximum value of 1.03 with  $\text{Co}_4\text{Sb}_{11.5}\text{Te}_{0.5}$  prepared under a pressure of 2.3 GPa.<sup>91</sup> In addition, researchers have attempted to dope Ba,<sup>92</sup> In,<sup>93</sup> Pb<sup>94</sup> or Sn<sup>95–97</sup> in  $\text{Co}_4\text{Sb}_{12-x}\text{Te}_x$ , and have made some progress in the increasing of the maximum *ZT* value. When  $\text{Ba}_{0.2}\text{Co}_4\text{Sb}_{11.5}\text{Te}_{0.5}$  was synthesized under a pressure of 3 GPa and at a temperature of 723 K, its maximum *ZT* value was 0.61. The  $\text{Pb}_{0.2}\text{Co}_4\text{Sb}_{11.5}\text{Te}_{0.5}$  sample prepared under the conditions of 3.5 GPa and 773 K had a power factor of  $27.3 \mu\text{W cm}^{-1} \text{K}^{-2}$ , a low thermal conductivity of  $2.26 \text{ W m}^{-1} \text{K}^{-1}$ , and a maximum *ZT* value of 0.93. After Sn doping, the highest *ZT* value of the  $\text{CoSb}_{2.75}\text{Te}_{0.20}\text{Sn}_{0.05}$  sample synthesized under 793 K and 3 GPa was 1.17.

By using the initial raw material  $\text{Mg}_2\text{Si}$ , researchers have tried to make another series of functional thermoelectric materials. Both Bi doping and Sb doping can improve the thermoelectric performance of  $\text{Mg}_2\text{Si}$ . When choosing the best ratio of compounds with different proportions, it is easy to find that the *ZT* value of  $\text{Mg}_2\text{Si}_{0.985}\text{Bi}_{0.015}$  is 0.98 at 773 K, which is higher than that of  $\text{Mg}_2\text{Si}_{0.985}\text{Sb}_{0.015}$  (0.94) at the same temperature.<sup>98,99</sup> Through Al doping, Bi and Sb exhibit the increase of point-defect phonon scattering, and  $\text{Mg}_{1.96}\text{Al}_{0.06}\text{Si}_{0.985}\text{Bi}_{0.01}\text{Sb}_{0.005}$  contributes the maximum *ZT* value of 0.9 at 773 K.<sup>100</sup>

### High-energy-density materials

In the last two decades, high-energy-density materials synthesized at high pressures have received significant attention due to their interesting chemical properties. High pressure can effectively destroy the strong triple bond in the nitrogen molecule to synthesize the polymeric nitrogen phase. These specimens release large amounts of energy when the single-bond/double-bond nitrogen in the condensed phase decomposes into triple-bonded inert gas-phase  $\text{N}_2$  molecules.<sup>101</sup> As part of the aryl pentazole molecule,  $\text{N}_5^-$  has been known since the mid-1950s, however it is still a hard task to synthesize solid-state compounds consisting of pentazolate anions  $\text{N}_5^-$ . Recently, researchers at the University of South Florida successfully synthesized a solid compound consisting of the isolated pentazolate anion  $\text{N}_5^-$ , which was obtained by compressing and laser heating a mixture of cesium azide ( $\text{CsN}_3$ ) and  $\text{N}_2$  cryogenic liquid in DAC.<sup>5</sup> Inspired by this research, some naked cyclic  $\text{N}_5^-$  salts were designed, such as  $\text{CuN}_5$ ,<sup>102</sup>  $\text{LiN}_5$ <sup>103</sup> and  $\text{SeN}_5$ .<sup>104</sup> By forming a stable metal pentazole hydrate through hydrogen bonding with water, such as the well-known  $[\text{LiNa}(\text{N}_5)_2(\text{H}_2\text{O})_4] \cdot \text{H}_2\text{O}$ ,<sup>105</sup>  $[\text{M}(\text{H}_2\text{O})_4(\text{N}_5)_2] \cdot 4\text{H}_2\text{O}$  ( $\text{M} = \text{Mn}, \text{Fe}, \text{Co}$  and  $\text{Zn}$ ),<sup>106</sup>  $[\text{Na}(\text{H}_2\text{O})(\text{N}_5)] \cdot 2\text{H}_2\text{O}$  and  $[\text{Mg}(\text{H}_2\text{O})_6(\text{N}_5)_2] \cdot 4\text{H}_2\text{O}$ ,<sup>107</sup> the exposed metal pentazolyl salt has a higher volume energy density and is considered to be an ideal high-energy-density material. By using the structure search method, in a study of the high-pressure phase diagram of the Zn–N system, Liu *et al.* proposed a metastable phase with an unconventional stoichiometric ratio,  $\text{P}\bar{\text{I}}\text{-ZnN}_6$ , and its energy density is  $2.72 \text{ kJ g}^{-1}$ , which is comparable to that of  $\text{LiN}_5$  ( $2.72 \text{ kJ g}^{-1}$ ). The pressure to maintain the stability of the metastable phase  $\text{P}\bar{\text{I}}\text{-ZnN}_6$  exceeds 100 GPa. The energy densities of another two newly proposed potential high-energy-density phases  $\text{P}\bar{\text{I}}\text{-ZnN}_4$

and  $\text{Ibam-ZnN}_4$  are  $2 \text{ kJ g}^{-1}$  and  $2.3 \text{ kJ g}^{-1}$ , respectively, and their stable pressure ranges are 16.9–91.39 GPa and 91.39–100 GPa, respectively.<sup>108</sup> It must be pointed out that the  $\text{LiN}_5$  compound is not only the first environmentally stable pentazo salt synthesized under high pressure, but also the poly-nitrogen compound with the highest nitrogen content at room temperature.

The structure search predicts new stoichiometries nitrides, such as  $\text{SrN}_5$  which is stable under ambient pressure up to 100 GPa,<sup>109</sup> while the  $\text{WN}_6$  crystal is thermodynamically stable at pressures above 16 GPa, but remains dynamically stable under ambient conditions.<sup>110</sup> In the  $\text{cyclo-N}_6^{6-}$  unit all nitrogen atoms are singly bonded and therefore contain a higher energy density compared with  $\text{N}_5^-$ , which has become the next generation of the research and development direction for high energy density materials.

### Semiconductor

Because the application of semiconductors in the field of electronics and photovoltaics continues to expand and pave the way for the development of optoelectronic devices, it is increasingly important in modern society. Most semiconductors consist of a network of covalent bonds and form an open crystal structure. Since this structure becomes denser when melting, semiconductors usually exhibit a series of high-pressure phase transitions, and gradually form a denser structure under the effect of high pressure.<sup>111</sup> The boron-doped diamond, synthesized from a powder mixture of detonation nano-diamond, pentaerythritol  $\text{C}_5\text{H}_8(\text{OH})_4$  and amorphous boron at a pressure of 7 GPa and a temperature of 1500 K, has an electrical conductivity of about  $0.2 \Omega^{-1} \text{ cm}^{-1}$ , which can be attributed to boron with a doping concentration of 0.1 atm%.<sup>112</sup> The Hall coefficient (an electromagnetic effect coefficient) of B and S doped diamond is inversely related to the element doping content, which indicates that the synthesized crystal is a n-type semiconductor. This is because during the dynamic equilibrium process, the extra electrons provided by the S donors make up for the vacancies created by B acceptors. Another explanation is that during the diamond crystallization process, the combination of B and S forms an integral composite donor.<sup>113</sup> When phosphorus is used to dope the diamond, the free electrons in the doped diamond are excessive, since the tetravalent carbon atoms are replaced by pentavalent phosphorus atoms. These results show that, with the increase of phosphorus content, the semiconductor properties of large diamond single crystals have been significantly improved.<sup>114</sup> The boron-doped single crystal diamond with a 1–1.5  $\mu\text{m}$  boron-rich layer has a shallow electron donor state and behaves as an n-type semiconductor, accompanied by a high carrier concentration ( $0.778 \times 10^{21} \text{ cm}^{-3}$ ) and high conductivity.<sup>115</sup> The dopant Y atom can not only greatly reduce the defect formation energy to generate more Cd vacancies, but also improve the magnetic properties of CdS with a wurtzite structure, and tend to form Cd vacancy defects in CdS with a rock-salt structure.<sup>6</sup> Nitride semiconductors are attractive because they can be environmentally benign and possess



favourable electronic properties.  $\text{CaZn}_2\text{N}_2$  is a new compound predicted by DFT and synthesized under high pressure. The variety in bandgaps of the identified compounds could expand the potential suitability of nitride semiconductors for a broader range of electronic, optoelectronic and photovoltaic applications.<sup>116</sup>

### Nano-diamond and doped diamond

**Synthesis of nano-diamond (ND).** When the size of the structural unit is reduced to below 100 nm, the material usually produces new characteristics. This phenomenon can be explained as follows. A considerable part of the atoms of the nanoparticle is on its surface, resulting in an increase of the surface free energy. Since the prospect for the nano-diamond synthesis at HPHT is mainly associated with the use of thermodynamically stable conditions, this is the most favorable for obtaining the perfect diamond structure. Unlike CVD technology, the structural hydrogen impurity is not detected in diamonds synthesized at high pressures, which is enough to prove that high pressure is irreplaceable in the field of diamond synthesis. The main studied types of syntheses and results obtained are given in Table 4. The hardness of ND exceeds that of single crystal diamond, thus showing high application expectations in various industrial instruments and scientific fields. If the synthesized [200]-faceted NDs are less than 1 nm in diameter, they will be kinetically stable up to 1500 K. In experiments conducted using pressure medium (such as  $\text{Na}_2\text{CO}_3$  and  $\text{NaCl}$ ) that is easily melted under the temperature and pressure conditions for ND synthesis, some carbon is dissolved in the hydraulic medium and recrystallized on the surface of the diamond balls, which is both a carbon source and a substrate. Instead, magnesium oxide ( $\text{MgO}$ ) can be used as a suitable pressure medium for converting solid glassy carbon to nanocrystalline diamond (NCD).<sup>117</sup> If the energy transferred to an atom in the lattice by high energy particles is larger than the displacement threshold energy, the atom is displaced into the lattice to form an interstitial, leaving a vacancy behind, which is called a Frenkel pair. At temperatures above 300 °C, Frenkel pairs will annihilate each other, forming structural defects. Many structural defects exist in the irradiated highly oriented pyrolytic graphite (HOPG), which provide preferential nucleation sites for the growth of cubic diamond. As a result, the formation of diamond mainly takes place through the nucleation and growth process.<sup>118</sup> The development of ND materials for quantum computing and sensing applications increasingly depends on the improvement of synthesis methods, so that the formation of point defects in the ND lattice can be precisely controlled. Using the CB $\Omega$  theory to model the vacancy, the temperature dependence of the nitrogen-vacancy ( $\text{NV}^-$ ) center diffusion is proved, indicating that the vacancy diffusion will drive the formation of  $\text{NV}^-$ .<sup>119</sup> Silicon-doped NDs were obtained by laser heating a carbon aerogel formed by pre-treatment of tetraethyl orthosilicate in a DAC using argon as the pressure transmission medium at a pressure in the range of 20–25 GPa. The successful incorporation of silicon into NDs illustrates the potential

impact of this carbon aerogel doping method on doped NDs without ion implantation (such as high-pressure metrology), which will provide an effective way to obtain more complex NDs.<sup>120</sup> In the DAC, halogen adamantane  $\text{C}_{10}\text{H}_{14}\text{Br}_2$  and  $\text{C}_{10}\text{H}_{15}\text{Cl}$  were used as the starting materials, respectively. At a pressure of 8 GPa, using a heating method that gradually increased in temperature, NDs were finally formed. The halogen element in the decomposition process of halogen adamantane inhibited the formation of graphite with unsaturated bonds, and stabilized the carbon cluster by  $\text{sp}^3$  hybridized carbon, which led to the nucleation and growth of diamond. The cage molecular structure of halogen adamantane and the chemical properties of specific halogen elements ensure the effective nucleation of diamonds and their slow growth in C–H–Br systems at temperatures up to 2000 K, which provide new directions for the controlled synthesis of NDs.<sup>121</sup> Under the conditions of pressure 9.4 GPa and temperature 1500–1700 K, using a mixture of tetraphenyl germane  $\text{C}_{24}\text{H}_{20}\text{Ge}$  and adamantane  $\text{C}_{10}\text{H}_{16}$  as reactants, the synthesis of Ge-doped NDs with an average crystal size of 50 nm on a large scale was achieved, which strongly suggests that using high pressure is still the most effective method for obtaining doped NDs.<sup>122</sup> Filiform defects were observed throughout the interior of diamonds synthesized using traditional rapid cooling technology. Finite element simulations showed that the distributions and magnitude of the von Mises stress (force of deformation per unit volume) inside the diamond at the end of the synthesis varied greatly. Gradient cooling technology can decrease the damage due to thermoelastic stress in diamonds. By prolonging the gradient cooling time, the crystalline quality of diamond increased, and the number of filiform defects and inner stresses in diamond decreased. Gradient cooling can provide ideas for reducing crystal defects in synthetic diamond.<sup>123</sup>

**Enhancement of diamond hardness.** A typical method to enhance the hardness of diamonds is to promote the nanocrystallization of diamonds. This can be explained that according to the Hall–Petch effect, the hardness of diamond increases as the grain size and/or twin thickness decrease to the nanometer level. In the synthesis experiment of nano twinned diamonds, researchers attempted to explain the existence of the minimum thickness of twinned crystals, and the results showed that the pressure-dependent transformation of the plastic deformation mechanism occurred under the critical synthesis pressure for nano twinned diamonds.<sup>124</sup> The direct transformation mechanism from onion-like precursors to nano twinned diamonds indicates that the martensite process (non-diffused crystal transformations occurring in metals and alloys) is strongly influenced by pressure–temperature conditions.<sup>125</sup> Moreover, in addition to the defects in onion-like carbon, stacking faults are also critical to the formation of twinned-crystal boundaries in the product.<sup>126</sup> Since the precursor for synthesizing nano-polycrystalline diamond was changed from graphite to onion-like carbon, its synthesis pressure was reduced from 15 GPa to 10 GPa.<sup>127</sup> Recently synthesized optically transparent microspheres composed of bulk



**Table 4** Source, classification, method, treatment pressure, temperature, time and results of diamond fabricated using the references mentioned in this article

| Source | Classification   | Method, treatment pressure, temperature and time                                | Results  |
|--------|--|---|--|
| 3      | Nanocrystalline diamond                                      | Placed into capsules made of h-BN, Re or Pt, 9–18 GPa, 1250–2000 °C, 1 or 5 min | Created static pressures above 1 TPa.  |
| 117    | Nanocrystalline diamond                                      | Placed into capsules made of h-BN, Re or Pt, 9–18 GPa, 1250–2000 °C, 1 or 5 min | Using MgO as a pressure medium, 15–40 μm fully optically transparent nanocrystalline diamond micro-balls were synthesized at 18 GPa, 1850–2000 °C.   |
| 118    | Nanopolycrystalline diamond                                  | Enclosed in a Ta capsule, 15–23 GPa, 1500–2300 °C, 20 min                       | NPDs with various crystalline structures can potentially be synthesized from neutron-irradiated HOPG by controlling the density and distribution of the defects introduced.                    |
| 119    | Nano-diamond   | Treatment with an Ar/liquid N <sub>2</sub> mixture, 16.3–21 GPa, 1370–1740 K    | Vacancy diffusion drives the formation of NV <sup>−</sup> .  |
| 120    | Si doped nano-diamond  | Treatment with an Ar/liquid N <sub>2</sub> mixture, 20–25 GPa, 1800–3000 K      | Carbon aerogel, as a general method to produce colorcenters in diamonds, can control generation of designer defects.   |
| 121    | Halogen adamantane doped nano-diamond                        | 8 GPa, 1400–2000 °C, 2 min  | A good candidate for producing nano-diamonds.  |
| 122    | Si, Ge and Sn doped nano- and microdiamond                   | Placed in Ti capsules, 8–9 GPa, 1500–1900 K, 2 min                              | Ge-Doped nano-diamonds with an average size of 50 nm were synthesized on a large scale.  |
| 123    | Diamond with Fe <sub>64</sub> Ni <sub>36</sub> as a catalyst | 5.5 GPa, 1250–1300 °C   | Gradient cooling technology can reduce crystal defects.  |
| 124    | Nanotwinned diamond  | 18–25 GPa, 1850–2000 °C   | Vickers hardness reaches 203.6 ± 12.0 GPa when the twin thickness is 5.0 ± 0.2 nm.   |
| 125    | Nanotwinned diamond  | Placed in an h-BN capsule, 15–25 GPa, 1600–1800 °C                              | Vickers hardness reaches 215 GPa at an applied load of 4.9 N.  |
| 126    | Nanotwinned diamond and nanopolycrystalline diamond          | 20 GPa, 2000–2300 °C, 2–30 min  | 180 GPa Vickers hardness for nanotwinned diamond at an applied load of 4.9 N.  |
| 127    | Nanopolycrystalline diamond                                  | Placed in a h-BN sleeve, 10–15 GPa, 1600–1800 °C, 1–10 min                      | Under an applied load of 4.9 N, the Vickers hardness of nanopolycrystalline diamond with 6.9 nm grain size is 167 ± 8 GPa.   |
| 129    | N doped detonation nano-diamonds                             | Treatment with alcohol, 7 GPa, 1300 °C, 10 s                                    | The introduction of ethanol to cause diamond coalescence can be used to control the sintering efficiency of diamond crystallites.  |
| 130    | Ge doped diamond   | Placed in a Mo sleeve, 6–7 GPa, 1500–1800 °C, 1–60 h                            | Discovered an unreported new optical center related to germanium impurities.   |
| 131    | Mg and Si doped diamond                                      | Placed in a Mo sleeve, 7.5 GPa, 1800 °C, 30 min                                 | Cooperative doping of different elements determined the morphology of diamond.   |
| 132    | B and N doped diamond  | 5–6 GPa, 1300–1650 °C, 15 min   | The synergistic doping of light elements is a key parameter to control the growth processes, morphology, and defect-and-impurity structure of the diamond crystals.                            |
| 133    | Mg and Ge doped diamond                                      | Placed in a Mo sleeve, 7 GPa, 1500–1900 °C, 10 min–36 h                         | The feasibility of the Mg–Ge system for growing bulk low-strain diamond doped with isotopically enriched germanium is demonstrated.  |
| 134    | S and B doped diamond  | 5.5 GPa, 1580 K, 20–24 h  | B–S co-doping had a trend to promote the electrical properties of n-type diamonds.   |
| 135    | Ni and B doped diamond                                       | 6.2–6.4 GPa, 1370–1410 °C   | Boron additive in N-rich diamonds can accelerate the formation of N <sup>+</sup> centers and have better crystallinity, but sharply limits the Hall mobility of p-type diamond semiconductors. |
| 136    | B and N doped diamond  | 5–6 GPa, 1490–1900 °C   | The change of the crystallization medium caused by the different B and N source additives leads to the difference in characterization of the synthesized diamond crystals.                     |

nanocrystalline diamonds, due to the unique microstructure of bulk nanocrystalline diamonds, have excellent yield strength (approximately 460 GPa at a confining pressure of approximately 70 GPa). The ultra-high hardness of nanocrystalline diamond microspheres can produce a static pressure of more than 1 TPa, so this nanocrystalline diamond ball is expected to be widely used in DAC.<sup>3</sup>

**Diamond doped by light elements.** One of the most valuable forms of diamond, ND, has been discussed above. Since the diamond synthesis mechanism has also been systematically

explained a few years ago (as shown in Fig. 4), no further detailed discussion will be done here, but the focus will be on the synthesis and performance of the new diamond. In the electron paramagnetic resonance (EPR) of N-doped diamond powder sintered at high pressure and high temperature, the appearance of ultrafine structures due to “paramagnetic nitrogen” can be explained by the directional attachment and coalescence of submicron and micron-scale diamond single crystals grown from N-doped diamond nanocrystals. Due to the introduction of ethanol of low molecular weight during the

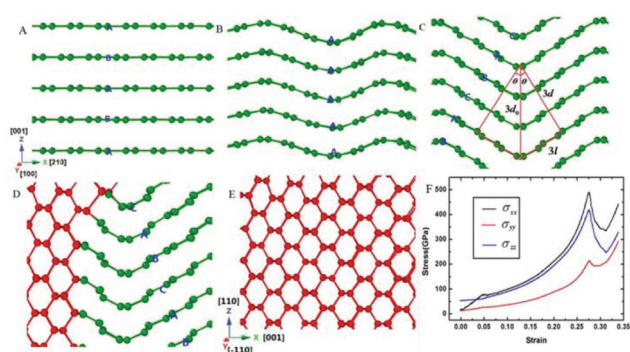


**Fig. 4** Transformation of hexagonal graphite with 0.240 nm interlayer distance into mono-crystal cubic diamond. In the figure, the green and red balls represent atoms that have three and four nearest neighbours, respectively. (A). The initial state of hexagonal graphite with 0.240 nm interlayer distance. (B). The wave-like buckling of the graphite layers leads to the stacking order of the graphite layers transforming from "ABAB" to "AAAA". (C). When the inclination angle reaches 30 u, the stacking order of the graphite transforming from "AAAA" to "ABCA" (rhombohedral graphite), and the interlayer distance (*d*) can be calculated as 0.208 nm. (D). Parts of graphite convert into cubic diamond. (E). Graphite completely transforms into single crystal cubic diamond. (F). The stress–strain curves in the compression process. Reproduced with permission from ref. 128. Copyright 2014, Nature.

experiment, diamond coalescence occurred. Theoretically, this mechanism can be used to control the sintering efficiency of diamond crystallites.<sup>129</sup>

**Diamond doped by semi-metals.** Under the conditions of a pressure of 6–7 GPa and a temperature of 1773–2073 K, using graphite rods as the starting material, germanium as the catalyst, and diamond (0.5 mm) as the seed crystal, after 1–60 hours of reaction time, the conversion rate of graphite-to-diamond can reach 90% to 95%, and diamond crystallizes through spontaneous nucleation and growth. The signal of the zero-phonon line (ZPL, the transition line from the lowest vibrational energy state of the excited state to the ground state) at 2.059 eV revealed a new optical center that was not previously reported, which is related to germanium impurities in diamond. The center of the Ge hole has weak electron coupling, and even at room temperature, it can produce photoluminescence in the relatively narrow spectral region of ZPL, thus potentially leading to many research topics relating to single photon and quantum optics applications. At this point, the chemical elements that can be incorporated into diamond to act as point defects are very limited. As a new optically active hole in diamond, the germanium hole expands the range of color center components, which is of great research value.<sup>130</sup> In the synthesis of diamonds through the Mg–Si–C system, it was observed that the morphology of the synthesized diamonds was determined by the amount of silicon incorporated into the diamonds. With the increase of Si content, the diamond has undergone a configuration change from cubic to octahedral, which is different from the synthetic system where the diamond morphology is determined mainly by the pressure–temperature parameters.<sup>131</sup> The presence of light

elements in the diamond synthesis system has a great influence on the properties of the catalyst, especially the solubility of carbon in the catalyst, so the morphology of diamond is mainly determined by the cooperative doping of different elements. To determine the shape of diamond, changing the growth conditions and morphology of diamond by adjusting the content of light elements can be considered.<sup>132</sup> When synthesizing diamond through the Mg–Ge–C system, Ge causes a decrease in the solubility of carbon in the catalyst, resulting in a decrease in the conversion rate and growth rate of diamond. Considering that the growth inhibitory effect occurs at low temperatures and the operating duration increases significantly, the diamond morphology changes may be related to the increasing of oxygen diffusion and melt viscosity.<sup>133</sup>

**Diamond doped by metals.** The n-type semiconductor diamond obtained by processing S/B–S co-doped FeNiCo–C at high temperature and high pressure shows a positive correlation between the increase in S or B dopant and the Hall mobility value. This trend indicates that the synthesis of large diamond crystals by B–S co-doping is an effective method to improve their electrical properties.<sup>134</sup> As the content of boron additive increases, the density of free carriers increases in the nitrogen-rich diamond system, and the resistivity and Hall mobility decrease. This shows that the n defect not only reduces the carrier density in B-doped semiconductor diamonds, but also severely limits the Hall mobility of the scattering center in the system.<sup>135</sup> The experimental results of FTIR and XPS demonstrate that in the experiment of synthesizing boron–nitrogen co-doped diamond by adding h–BN to the Fe–Ni–C system, a large number of C–C bonds were replaced by B–N bonds, and the diamond synthesized by the Fe–Ni–C–B–NaN<sub>3</sub> system is mainly composed of separated B-doped diamond and N-doped diamond. This indicates that under the synthesis conditions of BCN diamond with a pressure of 5.0–6.0 GPa and a temperature of 1490–1900 K, the chemical bond of B–N in BCN diamond obtained from the Fe–Ni–C–h–BN system is stronger than that in the BCN diamond obtained from the Fe–Ni–C–B–NaN<sub>3</sub> system.<sup>136</sup>

### Non-stoichiometric compounds

Non-stoichiometric compounds are ubiquitous worldwide, and high pressure is considered to be the most effective method for producing non-stoichiometric materials. Pressure can compress the outer electrons of atoms, thereby changing the fundamental properties of the elements, and thus it can lead to materials with unprecedented stoichiometries and chemical properties. To some extent, non-stoichiometric compounds are more important than stoichiometric compounds. When conducting high-pressure experiments, the sample is confined to a closed capsule, so high-pressure experiments can isolate environmental impurities from the sample, which is a unique advantage of high-pressure synthesis methods. At ambient pressure and temperature, both non-stoichiometric hcp hydride and fcc monohydride are unstable. Under a pressure higher than 45 GPa, CoH and a new dihydride CoH<sub>2</sub>

were synthesized using a mixture of Co and H<sub>2</sub> as the starting materials. This new dihydrogen compound CoH<sub>2</sub> can stably exist under a pressure of 10 GPa, and gradually decomposes to CoH as the pressure decreases, and finally decomposes completely below 3 GPa.<sup>137</sup> Under high-pressure conditions, compounds that are stable under normal pressure can also react with other substances to form completely new materials. The theoretical calculation results predict that Na<sub>2</sub>He compounds can exist stably under the pressure of 113 GPa, Xe<sub>2</sub>O<sub>5</sub> can exist stably under the oxygen-rich conditions and 83 GPa, Xe<sub>3</sub>O<sub>2</sub> can stably exist under the oxygen-poor conditions and 77 GPa.

Under certain pressure conditions, as the electron orbits will collapse to a certain extent, the outermost electrons of the inert element will become active, thereby activating the element, making it easy to combine with other substances, and resulting in some metal characteristics.<sup>8,158</sup> The Raman measurement results show that the prediction results of the metallicity of the magnesite FeN<sub>2</sub> do not match the measurement results of the non-metallicity, indicating that the theoretical prediction may be completely different from the actual situation under high pressure.<sup>159</sup> FeN<sub>4</sub> is also a high-energy-density material, but the high synthesis pressure still limits its practical application, so this synthesis can only promote the study of high energy nitrogen bonds to a certain extent.<sup>160</sup> A new type of nitrogen-rich compound ReN<sub>8</sub>·xN<sub>2</sub> was synthesized by directly reacting between rhenium and nitrogen at 134 GPa and 2700 (200) K in DAC, which is the inorganic compound with the highest nitrogen content known to date. Single-crystal X-ray diffraction revealed that the ReN<sub>8</sub> framework crystal structure has rectangular channels to accommodate nitrogen molecules, which is why ReN<sub>8</sub>·xN<sub>2</sub> is an inclusion compound.<sup>161</sup> Due to the existence of short incompressible B–B bonds, Fe<sub>2</sub>B<sub>7</sub> synthesized at 15 GPa has been regarded as a potential hard material. Another compound in the Fe–B system, Fe<sub>x</sub>B<sub>50</sub>, is synthesized under a pressure of 12 GPa, and it does not show obvious anisotropy in elastic behavior.<sup>162</sup> As Cs behaves like a 5p element, the well-established inertness of inner-shell electrons is not always observed at high pressure. In a similar circumstance, the reaction between K and Br<sub>2</sub> to generate KBr<sub>3</sub> and KBr<sub>5</sub> under high pressure indicates that electrons will transfer from the 4d inner shell of K to Br, so K will exhibit some of the characteristics of transition metals under pressure.<sup>163</sup>

### Some new phases and new materials synthesized by HTHP

Materials discovery is crucial for the continued exploration of emergent phenomena, including superconductivity and topological insulating behavior. However, the creation of new compounds *via* the traditional solid-state methodology has inherent limitations, as the high temperatures commonly employed select for the most thermodynamically stable product. By revising interatomic distances and bonding methods, high pressure can change the energy stability of various possible structures, thereby generating new materials through structural phase transitions. The extreme pressure

shifts the energy landscape such that new structures, not typically accessible using traditional solid-state modus, become thermodynamically stable at elevated pressure. Herein, a new high-pressure phase in the Ni–Bi system, β-NiBi, has been discovered, which crystallizes in the TII structure type. The powerful technique of *in situ* high-pressure and high-temperature powder X-ray diffraction enabled observation of the formation of β-NiBi under a pressure of 39.3 (1) GPa and a temperature of 973 K, and its reversible reconversion to the ambient pressure phase, α-NiBi.<sup>164</sup> Furthermore, high pressure can also be used in solid-state chemistry to stabilize the precursor by increasing its decomposition temperature. Under the atmospheric pressure conditions, the instability of silver oxide poses great challenges for the synthesis of AgGaO<sub>2</sub>. Through the solid phase reaction of Ag<sub>2</sub>O and Ga<sub>2</sub>O<sub>3</sub> powder, α-AgGaO<sub>2</sub> was successfully stabilized by the solid phase reaction of 10 GPa, which means that high pressure can modify existing materials and synthesize non-equilibrium phases or novel compounds.<sup>165</sup>

On the other hand, the morphology of the material will also play a crucial role in exploring emerging phenomena. Two-dimensional materials have significant potential for the development of new devices. For a small-band-gap semiconductor, black phosphorus (black-P) displays high mobility charge carriers and can easily be exfoliated. β-GeSe is made at 6 GPa and over 1000 K and is stable under ambient conditions. Due to their unique two-dimensional crystal structure, such as the unique electronic band gap of the β-GeSe polymorphic phase, these materials have great application potential.<sup>166</sup> In semiconductors, silicon is the most widely studied material. The electronic structures of most silicon allotropes are quite well understood; however, there remain numerous controversies, especially regarding the Si-III phase. With DAC, phase-pure samples of a metastable allotrope of silicon, Si-III or BC8, were synthesized by direct elemental transformation at 14 GPa and about 900 K and also at significantly reduced pressure in the Na–Si system at 9.5 GPa by quenching from approximately 1000 K, and this could help us to tackle challenges in electronic and photovoltaic applications.<sup>167</sup> Because of their remarkable mechanical properties, Mg-transition-metal (TM)-rare-earth (RE) alloys containing a synchronized long-period-stacking order (LPSO) structure have received significant attention. Unexpectedly, under high pressure (5 GPa) and high temperature (723 K), a new type of long-period superlattice Mg<sub>77</sub>Zn<sub>9</sub>Yb<sub>14</sub> was found in Mg<sub>97</sub>ZnYb<sub>2</sub> alloys. This research provides magnesium alloys with the potential as a lightweight structural material to replace aluminum alloys.<sup>168</sup>

Finally, since more than 95% of substances inside the Earth is in a high-pressure state of at least 10 GPa, high-pressure science and earth science theory have an inseparable relationship. In other words, the new phases of the compounds and the new compounds may become the key tracking substances in earth science. For instance, at different ground depths, Fe<sub>2</sub>O<sub>3</sub> will have a profound effect on the Earth's magnetic field. Therefore, it has become a key factor in studying the movement of rocks inside the Earth (Fig. 5).

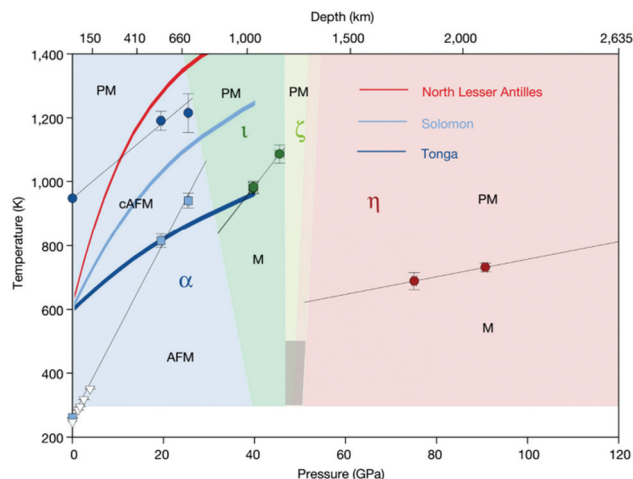


**Fig. 5** Magnetic phase diagram of  $\text{Fe}_2\text{O}_3$ . The magnetic critical temperatures at high pressure from this study and the Néel and Morin temperatures at ambient pressure are denoted by filled symbols. Temperatures of the Morin transition below 4 GPa from the neutron-diffraction studies are marked by empty triangles. Black solid lines are linear fits to the data. The dark-shaded region in the stability field of  $\zeta\text{-Fe}_2\text{O}_3$  indicates the possible range of the critical temperature for this phase. Coloured lines show the pressure–temperature profiles for subducting slabs. We note that  $\alpha\text{-Fe}_2\text{O}_3$  remains magnetic down to transition-zone depths in very cold (Tonga) and cold (Solomon) subducting slabs. PM, paramagnetic; AFM, antiferromagnetic; cAFM, antiferromagnetic with spin canting; M, magnetic with unknown longrange magnetic order. The crystallographic designation of the phases is provided in the main text. Both horizontal and vertical error bars are one standard error. Reproduced with permission from ref. 169. Copyright 2019, Nature.

In addition, many studies have shown that new materials can be efficiently synthesized under high pressure (see Table 5), such as composite materials, nanocrystals or high-entropy alloys. These materials are expected to be applied in different fields and provide some inspiration for the synthesis of new materials in the future.

## Conclusions

High pressure synthesis has reached many breakthroughs in the past five years, which demonstrates that high pressure synthesis is still the most effective tool to create new materials. Compared with normal atoms, the arrangement of atoms under high pressure is closer, and the chance of contact between different atoms at the microscopic level is increased, which may explain why many materials can be synthesized under high pressure but not under normal conditions. In this review, we classify the materials according to their properties and discuss their synthesis mechanism. Hydrogen-rich materials have significantly increased the  $T_c$  of superconducting materials, which not only means that researchers have approached the dream of superconducting at room temperature, but also urges scientists to further study and promote the development of superconducting theory. The 1 TPa hydrostatic

pressure reached by nanocrystalline diamond increases the pressure limit created by scientists and also provides the possibility of achieving the synthesis under higher pressure. The successful synthesis of penta-nitrogen salts means that great progress has been made in the direction of high-energy-density materials, and the discovery of new phases of materials and the synthesis of new substances have greatly deepened people's understanding of materials. These breakthroughs have made outstanding contributions to exploring new materials and discovering new properties, and provided specific guidance for high-pressure synthesis. There is no doubt that high-pressure synthesis will continue to provide more scientifically significant research results in the future.

## Conflicts of interest

There are no conflicts to declare.

## Acknowledgements

This work was supported by the National Natural Science Foundation of China (no. 21271082 and 21371068).

## Notes and references

- 1 J. P. Walsh and D. E. Freedman, High-pressure synthesis: A new frontier in the search for next-generation intermetallic compounds, *Acc. Chem. Res.*, 2018, **51**, 1315–1323.
- 2 Z. M. Geballe, H. Liu, A. K. Mishra, M. Ahart, M. Somayazulu, Y. Meng, M. Baldini and R. J. Hemley, Synthesis and stability of lanthanum superhydrides, *Angew. Chem., Int. Ed.*, 2018, **57**, 688–692.
- 3 N. Dubrovinskaia, L. Dubrovinsky, N. A. Solopova, A. Abakumov, S. Turner, M. Hanfland, E. Bykova, M. Bykov, C. Prescher and V. B. Prakapenka, Terapascal static pressure generation with ultrahigh yield strength nanodiamond, *Sci. Adv.*, 2016, **2**, e1600341.
- 4 J. Leszczyński, W. Szczypka, C. Candolfi, A. Dauscher, B. Lenoir and A. Koleżyński, HPHT synthesis of highly doped  $\text{In}_x\text{Co}_4\text{Sb}_{12-x}$  Experimental and theoretical study, *J. Alloys Compd.*, 2017, **727**, 1178–1188.
- 5 B. A. Steele, E. Stavrou, J. C. Crowhurst, J. M. Zaug, V. B. Prakapenka and I. I. Oleynik, High-pressure synthesis of a pentazolate salt, *Chem. Mater.*, 2016, **29**, 735–741.
- 6 P. Wang, B. Xiao, R. Zhao, Y. Ma and M. Zhang, Structure-Dependent Spin Polarization in Polymorphic CdS: Y Semiconductor Nanocrystals, *ACS Appl. Mater. Interfaces*, 2016, **8**, 6656–6661.
- 7 E. M. Smith and W. Wang, Fluid  $\text{CH}_4$  and  $\text{H}_2$  trapped around metallic inclusions in HPHT synthetic diamond, *Diamond Relat. Mater.*, 2016, **68**, 10–12.
- 8 X. Dong, A. R. Oganov, A. F. Goncharov, E. Stavrou, S. Lobanov, G. Saleh, G.-R. Qian, Q. Zhu, C. Gatti and



**Table 5** Some new phases and new materials synthesized under high-pressure and high-temperature conditions

| Year | Pressure (GPa) | Temperature (K) | Phase/material   | Brief description  | Ref. |
|------|----------------|-----------------|--|--|------|
| 2017 | 4              | 973             | Rossmannitic tourmaline  | First synthesis of rossmanitic tourmaline.   | 138  |
| 2018 | 4.7            | 2000            | MnC  | First time formation of novel manganese monocarbide (MnC).   | 139  |
| 2016 | 5.2            | 190             | Polyacetylene/ZSM-22   | Novel organic/inorganic subnanocomposite materials made of 1D guest polymers.  | 140  |
| 2015 | 5.5            | 1523            | Mn <sub>2</sub> ScSbO <sub>6</sub>   | Two new cation-ordered polymorphs of Mn <sub>2</sub> ScSbO <sub>6</sub>  | 141  |
| 2015 | 6              | 1373–1573       | CdMn <sub>7</sub> O <sub>12</sub> perovskites  | Structural phase transitions at 493 K in CdMn <sub>7</sub> O <sub>12</sub> .   | 142  |
| 2015 | 6              | 1373–1573       | SrMn <sub>7-x</sub> Fe <sub>x</sub> O <sub>12</sub> ( $x = 0, 0.08,$ and $0.5$ ) perovskites | Structural phase transitions at 404 K in SrMn <sub>7</sub> O <sub>12</sub> .   | 143  |
| 2017 | 6              | 1673            | 6M perovskite SrRhO <sub>3</sub>   | A new 6M polytype of SrRhO <sub>3</sub> stabilized under HTHP conditions   | 143  |
| 2019 | 6              | 1570            | Tl <sub>2</sub> NiMnO <sub>6</sub>   | A relatively ordered double perovskite.  | 144  |
| 2020 | 6.5–10.5       | 2123            | <i>Pnma</i> -SeC   | A new phase of carbon-selenium compound.   | 145  |
| 2015 | 7              | 77              | Polycarbonyl   | Entirely new type of polymers.   | 146  |
| 2016 | 7–10           | 77              | Polycarbonyl/ZSM-22  | Novel organic/inorganic subnanocomposite materials made of 1D guest polymers.  | 141  |
| 2015 | 7.5            | 1273            | PbZnO <sub>3</sub>   | A novel LiNbO <sub>3</sub> -type (LN-type) lead zinc oxide, PbZnO <sub>3</sub>   | 147  |
| 2015 | 8              | 2000            | Hexagonal Os <sub>2</sub> C  | Os <sub>2</sub> C is synthesized for the first time by the HPHT route using the laser heated diamond anvil cell (LHDAC) technique.             | 148  |
| 2017 | 8.5            | —               | CdSe/CdS-Au hetero-dimers nanocrystals   | Provides a fundamental understanding of the pressure-driven HNC-SL transformations at the atomic scale.  | 9    |
| 2019 | 9              | —               | <i>C2/m</i> -TaN <sub>2</sub>  | A new phase of TaN <sub>2</sub> .  | 149  |
| 2018 | 12             | 1473            | Co <sub>0.6</sub> Fe <sub>3.4</sub> O <sub>5</sub>   | New ferrite MFe <sub>3</sub> O <sub>5</sub> family   | 150  |
| 2018 | 13             | —               | CoCrFeMnNi high-entropy alloy  | Bulk CoCrFeMnNi high-entropy alloy with a hcp $\epsilon$ -martensite phase, and the fcc-to-hcp phase transition occurs at 13 GPa.              | 151  |
| 2017 | 14             | 340             | CrMnFeCoNi high-entropy alloy  | CrMnFeCoNi high-entropy alloy with the fcc-to-hcp phase transition occurs at 14 GPa.   | 152  |
| 2017 | 15.8           | —               | CdSe/CdS-Au hetero-rods nanocrystals   | Provides a fundamental understanding of the pressure-driven HNC-SL transformations at the atomic scale.  | 9    |
| 2020 | 18.3           | —               | <i>P2<sub>1</sub>/m</i> -CaN <sub>4</sub>  | A new HTHP phase of CaN <sub>4</sub> with the <i>P2<sub>1</sub>/m</i> space group.   | 153  |
| 2018 | 27.5           | 1696            | Li zigzag graphene nanoribbons LiC <sub>2</sub>  | Control graphene nanoribbons' electronic transport properties with a particular edge type and width.   | 154  |
| 2019 | 33             | 2273            | Re <sub>2</sub> (N <sub>2</sub> )(N) <sub>2</sub>  | A new high-pressure nitrogen-rich phase in the Re-N system.  | 155  |
| 2018 | 36.5           | 2010            | Li zigzag graphene nanoribbons Li <sub>3</sub> C <sub>4</sub>                                | Control graphene nanoribbons' electronic transport properties with a particular edge type and width.   | 154  |
| 2019 | 65             | —               | <i>Cmce</i> -TaN <sub>2</sub>  | A new phase of TaN <sub>2</sub> .  | 149  |
| 2016 | 73             | 2400            | TiN <sub>2</sub>   | A new transition metal pernitride, TiN <sub>2</sub> , has been synthesized.  | 156  |
| 2020 | 200            | 3000            | Hexagonal <i>hP</i> -ReC and orthorhombic <i>oF</i> -ReC <sub>2</sub>                        | Two novel carbon-rich rhenium carbides: WC-type structured <i>hP</i> -ReC and TiSi <sub>2</sub> -type structured <i>oF</i> -ReC <sub>2</sub> . | 157  |

- V. L. Deringer, A stable compound of helium and sodium at high pressure, *Nat. Chem.*, 2017, **9**, 440–445.
- 9 H. Zhu, Y. Nagaoka, K. Hills-Kimball, R. Tan, L. Yu, Y. Fang, K. Wang, R. Li, Z. Wang and O. Chen, Pressure-enabled synthesis of hetero-dimers and hetero-rods through intraparticle coalescence and interparticle fusion of quantum-dot-Au satellite nanocrystals, *J. Am. Chem. Soc.*, 2017, **139**, 8408–8411.
- 10 H. Hosono and K. Kuroki, Iron-based superconductors: Current status of materials and pairing mechanism, *Physica C*, 2015, **514**, 399–422.
- 11 H. M. Syed, C. Webb and E. M. Gray, Hydrogen-modified superconductors: A review, *Prog. Solid State Chem.*, 2016, **44**, 20–34.
- 12 S. Brown, Organic superconductors: The Bechgaard salts and relatives, *Physica C*, 2015, **514**, 279–289.
- 13 A. F. Goncharov and R. Hemley, Probing hydrogen-rich molecular systems at high pressures and temperatures, *Chem. Soc. Rev.*, 2006, **35**, 899–907.
- 14 Y. L. Godec, A. Courac and V. L. Solozhenko, High-pressure synthesis of ultrahard materials, *J. Appl. Phys.*, 2019, **126**, 151102.
- 15 Y. Tian, B. Xu and Z. Zhao, Microscopic theory of hardness and design of novel superhard crystals, *Int. J. Refract. Met. Hard Mater.*, 2012, **33**, 93–106.
- 16 W. Liu and S. Bai, Thermoelectric interface materials: A perspective to the challenge of thermoelectric power generation module, *J. Materiomics*, 2019, **5**, 321–336.
- 17 F. P. Fabbiani and C. R. Pulham, High-pressure studies of pharmaceutical compounds and energetic materials, *Chem. Soc. Rev.*, 2006, **35**, 932–942.
- 18 E. Horvath-Bordon, R. Riedel, A. Zerr, P. F. McMillan, G. Auffermann, Y. Prots, W. Bronger, R. Kniep and P. Kroll, High-pressure chemistry of nitride-based materials, *Chem. Soc. Rev.*, 2006, **35**, 987–1014.
- 19 M. Schreck, M. Mayr, O. Klein, M. Fischer, S. Gsell, A. F. Sartori and B. C. Gallheber, Multiple role of dislocations in the heteroepitaxial growth of diamond: A brief review, *Phys. Status Solidi*, 2016, **213**, 2028–2035.
- 20 R. Khmel'nitskiy, Prospects for the synthesis of large single-crystal diamonds, *Phys.-Usp.*, 2015, **58**, 134–149.
- 21 V. Lysakovskiy, N. Novikov, S. Ivakhnenko, O. Zanevskyy and T. Kovalenko, Growth of Structurally Perfect Diamond

- Single Crystals at High Pressures and Temperatures. Review, *J. Superhard Mater.*, 2018, **40**, 315–324.
- 22 V. Nadolinny, A. Komarovskikh and Y. Palyanov, Incorporation of large impurity atoms into the diamond crystal lattice: EPR of split-vacancy defects in diamond, *Crystals*, 2017, **7**, 237.
  - 23 E. A. Ekimov and M. V. Kondrin, Vacancy-impurity centers in diamond: prospects for synthesis and applications, *Phys.-Usp.*, 2017, **60**, 539–558.
  - 24 N. Yang, S. Yu, J. V. Macpherson, Y. Einaga, H. Zhao, G. Zhao, G. M. Swain and X. Jiang, Conductive diamond: synthesis, properties, and electrochemical applications, *Chem. Soc. Rev.*, 2019, **48**, 157–204.
  - 25 O. A. Shenderova, A. I. Shames, N. A. Nunn, M. D. Torelli, I. Vlasov and A. Zaitsev, Synthesis, properties, and applications of fluorescent diamond particles, *J. Vac. Sci. Technol., B*, 2019, **37**, 030802.
  - 26 H. Lai, M. Stenzel and P. Xiao, Surface engineering and applications of nanodiamonds in cancer treatment and imaging, *Int. Mater. Rev.*, 2020, **65**, 189–225.
  - 27 P. Karami, S. S. Khasraghi, M. Hashemi, S. Rabiei and A. Shojaei, Polymer/nanodiamond composites-a comprehensive review from synthesis and fabrication to properties and applications, *Adv. Colloid Interface Sci.*, 2019, **269**, 122–151.
  - 28 N. Yang, X. Jiang and D.-W. Pang, *Carbon nanoparticles and nanostructures*, Springer, Cham, 2016.
  - 29 N. Yang, J. S. Foord and X. Jiang, Diamond electrochemistry at the nanoscale: A review, *Carbon*, 2016, **99**, 90–110.
  - 30 S. Kumar, M. Nehra, D. Kedia, N. Dilbaghi, K. Tankeshwar and K.-H. Kim, Nanodiamonds: Emerging face of future nanotechnology, *Carbon*, 2019, **143**, 678–699.
  - 31 D. J. Garrett, W. Tong, D. A. Simpson and H. Meffin, Diamond for neural interfacing: a review, *Carbon*, 2016, **102**, 437–454.
  - 32 N. Nunn, M. Torelli, G. McGuire and O. Shenderova, Nanodiamond: a high impact nanomaterial, *Curr. Opin. Solid State Mater. Sci.*, 2017, **21**, 1–9.
  - 33 C. Buzea and K. Robbie, Assembling the puzzle of superconducting elements: a review, *Supercond. Sci. Technol.*, 2004, **18**, R1–R8.
  - 34 J. Hamlin, Superconductivity in the metallic elements at high pressures, *Physica C*, 2015, **514**, 59–76.
  - 35 K. Shimizu, H. Ishikawa, D. Takao, T. Yagi and K. Amaya, Superconductivity in compressed lithium at 20 K, *Nature*, 2002, **419**, 597–599.
  - 36 O. Prakash, A. Kumar, A. Thamizhavel and S. Ramakrishnan, Evidence for bulk superconductivity in pure bismuth single crystals at ambient pressure, *Science*, 2017, **355**, 52–55.
  - 37 Y.-G. Lu, S. Turner, E. Ekimov, J. Verbeeck and G. Van Tendeloo, Boron-rich inclusions and boron distribution in HPHT polycrystalline superconducting diamond, *Carbon*, 2015, **86**, 156–162.
  - 38 E. Ekimov, V. Sidorov, K. Maslakov, B. Sirotinkin, M. Krotova and Y. V. Pleskov, Influence of growth medium composition on the incorporation of boron in HPHT diamond, *Diamond Relat. Mater.*, 2018, **89**, 101–107.
  - 39 E. A. Ekimov, O. S. Kudryavtsev, A. A. Khomich, O. I. Lebedev, T. A. Dolenko and I. I. Vlasov, High-Pressure Synthesis of Boron-Doped Ultrasmall Diamonds from an Organic Compound, *Adv. Mater.*, 2015, **27**, 5518–5522.
  - 40 W. Liu, H. Lin, R. Kang, X. Zhu, Y. Zhang, S. Zheng and H.-H. Wen, Magnetization of potassium-doped p-terphenyl and p-quaterphenyl by high-pressure synthesis, *Phys. Rev. B: Condens. Matter Mater. Phys.*, 2017, **96**, 224501.
  - 41 Y. Kawamura, S. Deminami, L. Salamakha, A. Sidorenko, P. Heinrich, H. Michor, E. Bauer and C. Sekine, Filled skutterudite superconductor  $\text{CaOs}_4\text{P}_{12}$  prepared by high-pressure synthesis, *Phys. Rev. B: Condens. Matter Mater. Phys.*, 2018, **98**, 024513.
  - 42 S. Ma, K. Bao, Q. Tao, L. Li, Y. Huang, X. Huang, Y. Zhao, C. Xu, P. Zhu and T. Cui, Revealing the Unusual Rigid Boron Chain Substructure in Hard and Superconductive Tantalum Monoboride, *Chem. – Eur. J.*, 2019, **25**, 5051–5057.
  - 43 A. G. Kvashnin, I. A. Kruglov, D. V. Semenov and A. R. Oganov, Iron superhydrides  $\text{FeH}_5$  and  $\text{FeH}_6$ : stability, electronic properties, and superconductivity, *J. Phys. Chem. C*, 2018, **122**, 4731–4736.
  - 44 A. Majumdar, S. T. John, M. Wu and Y. Yao, Superconductivity in  $\text{FeH}_5$ , *Phys. Rev. B: Condens. Matter Mater. Phys.*, 2017, **96**, 201107.
  - 45 H. Zhang, X. Jin, Y. Lv, Q. Zhuang, Y. Li, K. Bao, D. Li, B. Liu and T. Cui, Pressure-induced phase transition of  $\text{SnH}_4$ : a new layered structure, *RSC Adv.*, 2016, **6**, 10456–10461.
  - 46 Y. Ma, D. Duan, Z. Shao, D. Li, L. Wang, H. Yu, F. Tian, H. Xie, B. Liu and T. Cui, Prediction of superconducting ternary hydride  $\text{MgGeH}_6$ : from divergent high-pressure formation routes, *Phys. Chem. Chem. Phys.*, 2017, **19**, 27406–27412.
  - 47 S. Qian, X. Sheng, X. Yan, Y. Chen and B. Song, Theoretical study of stability and superconductivity of  $\text{ScH}_n$  ( $n = 4-8$ ) at high pressure, *Phys. Rev. B: Condens. Matter Mater. Phys.*, 2017, **96**, 094513.
  - 48 X. Feng, J. Zhang, G. Gao, H. Liu and H. Wang, Compressed sodalite-like  $\text{MgH}_6$  as a potential high-temperature superconductor, *RSC Adv.*, 2015, **5**, 59292–59296.
  - 49 A. G. Kvashnin, D. V. Semenov, I. A. Kruglov, I. A. Wrona and A. R. Oganov, High-temperature superconductivity in a Th–H system under pressure conditions, *ACS Appl. Mater. Interfaces*, 2018, **10**, 43809–43816.
  - 50 P. Kong, V. Minkov, M. Kuzovnikov, S. Besedin, A. Drozdov, S. Mozaffari, L. Balicas, F. Balakirev, V. Prakapenka and E. Greenberg, Superconductivity up to 243 K in yttrium hydrides under high pressure, 2019, arXiv preprint arXiv:10482.

- 51 H. Wang, S. T. John, K. Tanaka, T. Iitaka and Y. Ma, Superconductive sodalite-like clathrate calcium hydride at high pressures, *Proc. Natl. Acad. Sci., India, Sect. A*, 2012, **109**, 6463–6466.
- 52 D. V. Semenov, A. G. Kvashnin, I. A. Kruglov and A. R. Oganov, Actinium hydrides  $\text{AcH}_{10}$ ,  $\text{AcH}_{12}$ , and  $\text{AcH}_{16}$  as high-temperature conventional superconductors, *J. Phys. Chem. Lett.*, 2018, **9**, 1920–1926.
- 53 S. M. Clarke, J. P. Walsh, M. Amsler, C. D. Malliakas, T. Yu, S. Goedecker, Y. Wang, C. Wolverton and D. E. Freedman, Discovery of a Superconducting Cu-Bi Intermetallic Compound by High-Pressure Synthesis, *Angew. Chem., Int. Ed.*, 2016, **55**, 13446–13449.
- 54 S. M. Clarke, M. Amsler, J. P. Walsh, T. Yu, Y. Wang, Y. Meng, S. D. Jacobsen, C. Wolverton and D. E. Freedman, Creating binary Cu-Bi compounds via high-pressure synthesis: a combined experimental and theoretical study, *Chem. Mater.*, 2017, **29**, 5276–5285.
- 55 R. P. Dias and I. F. Silvera, Observation of the Wigner-Huntington transition to metallic hydrogen, *Science*, 2017, **355**, 715–718.
- 56 P. Loubeyre, F. Occelli and P. Dumas, Observation of a first order phase transition to metal hydrogen near 425 GPa, 2019, arXiv preprint arXiv:1906.05634.
- 57 V. V. Struzhkin, D. Y. Kim, E. Stavrou, T. Muramatsu, H.-k. Mao, C. J. Pickard, R. J. Needs, V. B. Prakapenka and A. F. Goncharov, Synthesis of sodium polyhydrides at high pressures, *Nat. Commun.*, 2016, **7**, 12267.
- 58 I. A. Kruglov, A. G. Kvashnin, A. F. Goncharov, A. R. Oganov, S. S. Lobanov, N. Holtgrewe, S. Jiang, V. B. Prakapenka, E. Greenberg and A. V. Yanilkin, Uranium polyhydrides at moderate pressures: Prediction, synthesis, and expected superconductivity, *Sci. Adv.*, 2018, **4**, eaat9776.
- 59 A. Drozdov, P. Kong, V. Minkov, S. Besedin, M. Kuzovnikov, S. Mozaffari, L. Balicas, F. Balakirev, D. Graf and V. Prakapenka, Superconductivity at 250 K in lanthanum hydride under high pressures, *Nature*, 2019, **569**, 528–531.
- 60 C. Pépin, G. Geneste, A. Dewaele, M. Mezouar and P. Loubeyre, Synthesis of  $\text{FeH}_5$ : A layered structure with atomic hydrogen slabs, *Science*, 2017, **357**, 382–385.
- 61 X. Li, X. Huang, D. Duan, C. J. Pickard, D. Zhou, H. Xie, Q. Zhuang, Y. Huang, Q. Zhou and B. Liu, Polyhydride  $\text{CeH}_9$  with an atomic-like hydrogen clathrate structure, *Nat. Commun.*, 2019, **10**, 1–7.
- 62 A. Machida, H. Saitoh, T. Hattori, A. Sano-Furukawa, K.-i. Funakoshi, T. Sato, S.-i. Orimo and K. Aoki, Hexagonal close-packed iron Hydride behind the conventional phase Diagram, *Sci. Rep.*, 2019, **9**, 1–9.
- 63 N. P. Salke, M. M. D. Esfahani, Y. Zhang, I. A. Kruglov, J. Zhou, Y. Wang, E. Greenberg, V. B. Prakapenka, J. Liu and A. R. Oganov, Synthesis of clathrate cerium superhydride  $\text{CeH}_9$  at 80–100 GPa with atomic hydrogen sublattice, *Nat. Commun.*, 2019, **10**, 1–10.
- 64 F. Peng, Y. Sun, C. J. Pickard, R. J. Needs, Q. Wu and Y. Ma, Hydrogen clathrate structures in rare earth hydrides at high pressures: possible route to room-temperature superconductivity, *Phys. Rev. Lett.*, 2017, **119**, 107001.
- 65 D. Zhou, D. V. Semenov, D. Duan, H. Xie, W. Chen, X. Huang, X. Li, B. Liu, A. R. Oganov and T. Cui, Superconducting praseodymium superhydrides, *Sci. Adv.*, 2020, **6**, eaax6849.
- 66 S. Ma, K. Bao, Q. Tao, C. Xu, X. Feng, X. Zhao, Y. Ge, P. Zhu and T. Cui, Double-zigzag boron chain-enhanced Vickers hardness and manganese bilayers-induced high d-electron mobility in  $\text{Mn}_3\text{B}_4$ , *Phys. Chem. Chem. Phys.*, 2019, **21**, 2697–2705.
- 67 C. Wang, Q. Tao, S. Dong, X. Wang and P. Zhu, Synthesis and mechanical character of hexagonal phase  $\delta$ -WN, *Inorg. Chem.*, 2017, **56**, 3970–3975.
- 68 H. Liang, F. Peng, H. Chen, L. Tan, Q. Zhang, C. Fan, S. Guan, X. Ni, A. Liang and X. Yan, High-pressure sintering of bulk  $\text{MoSi}_2$ : Microstructural, physical properties and mechanical behavior, *Mater. Sci. Eng., A*, 2018, **711**, 389–396.
- 69 P. Wang, R. Kumar, E. M. Sankaran, X. Qi, X. Zhang, D. Popov, A. L. Cornelius, B. Li, Y. Zhao and L. Wang, Vanadium diboride ( $\text{VB}_2$ ) synthesized at high pressure: elastic, mechanical, electronic, and magnetic properties and thermal stability, *Inorg. Chem.*, 2018, **57**, 1096–1105.
- 70 Z. Hou, H. Wang, Y.-n. Yang, X. Song, S. Chen, S. Wan, X. Zhao, M. Shang and B. Chen, High-pressure synthesis of high-performance submicron-sized polycrystalline  $\beta$ - $\text{Si}_3\text{N}_4$  bulk without additives, *Ceram. Int.*, 2020, **46**, 12449–12457.
- 71 C. Wang, L. Song and Y. Xie, Mechanical and Electrical Characteristics of  $\text{WB}_2$  Synthesized at High Pressure and High Temperature, *Materials*, 2020, **13**, 1212.
- 72 G. Rogl, M. J. Zehetbauer and P. F. Rogl, The Effect of Severe Plastic Deformation on Thermoelectric Performance of Skutterudites, Half-Heuslers and Bi-Tellurides, *Mater. Trans.*, 2019, **60**, 2071–2085.
- 73 B. Liu, X. Jia, H. Sun, B. Sun, Y. Zhang, H. Liu, L. Kong, D. Huo and H. Ma, HPHT synthesis, structure and electrical properties of type-I clathrates  $\text{Ba}_8\text{Al}_x\text{Si}_{46-x}$ , *J. Solid State Chem.*, 2016, **233**, 363–367.
- 74 B. Liu, X. Jia, D. Huo, H. Sun, Y. Zhang, B. Sun, H. Liu, L. Kong and H. Ma, Evolution of thermoelectric properties of substituted Si-based clathrates prepared by HPHT, *J. Alloys Compd.*, 2016, **666**, 93–97.
- 75 B. Sun, X. Jia, D. Huo, H. Sun, Y. Zhang, B. Liu, H. Liu, L. Kong and H. Ma, Rapid synthesis and effect of high temperature and high pressure processing on the structure and thermoelectric properties of clathrate  $\text{Ba}_8\text{Cu}_6\text{Si}_{16}\text{Ge}_{24}$ , *J. Alloys Compd.*, 2016, **658**, 19–22.
- 76 B. Sun, X. Jia, D. Huo, H. Sun, Y. Zhang, B. Liu, H. Liu, L. Kong, B. Liu and H. Ma, Rapid synthesis and enhanced thermoelectric properties of  $\text{Ba}_8\text{Cu}_6\text{Ge}_{8x}\text{Si}_{40-8x}$  ( $x = 0, 1, 2$ ,

- 3) alloys prepared using high-temperature, high-pressure method, *J. Alloys Compd.*, 2016, **681**, 374–378.
- 77 B. Liu, H. Ma, D. Huo, H. Liu, B. Liu and X. Jia, The effect of europium on structure and thermoelectric properties of silicon clathrates by HPHT synthesis, *Mater. Chem. Phys.*, 2018, **205**, 84–89.
- 78 B. Liu, H. Ma, D. Huo, H. Liu, B. Liu, J. Chen and X. Jia, Thermoelectric properties of In-substituted Ge-based clathrates prepared by HPHT, *J. Materiomics*, 2018, **4**, 68–74.
- 79 B. Sun, X. Jia, J. Zhao, Y. Li, H. Liu and H. Ma, Effects of pressure on the microstructure and simultaneous optimization of the electrical and thermal transport properties of  $\text{Yb}_{0.5}\text{Ba}_{7.5}\text{Ga}_{16}\text{Ge}_{30}$ , *Inorg. Chem.*, 2018, **57**, 3323–3328.
- 80 Y. Kang, Q. Zhang, C. Fan, W. Hu, C. Chen, L. Zhang, F. Yu, Y. Tian and B. Xu, High pressure synthesis and thermoelectric properties of polycrystalline  $\text{Bi}_2\text{Se}_3$ , *J. Alloys Compd.*, 2017, **700**, 223–227.
- 81 Y. Zhang, X. Jia, H. Sun, B. Sun, B. Liu, H. Liu, L. Kong and H. Ma, Suppressing adverse intrinsic conduction of  $\text{Bi}_2\text{Te}_3$  thermoelectric bulks by Sb and Cu co-substitutions via HPHT synthesis, *RSC Adv.*, 2016, **6**, 7378–7383.
- 82 X. Guo, J. Qin, X. Jia, H. Ma and H. Jia, Quaternary thermoelectric materials: Synthesis, microstructure and thermoelectric properties of the  $(\text{Bi}, \text{Sb})_2(\text{Te}, \text{Se})_3$  alloys, *J. Alloys Compd.*, 2017, **705**, 363–368.
- 83 Y. Zhang, X. Jia, H. Sun, B. Sun, B. Liu, H. Liu, L. Kong and H. Ma, Enhanced thermoelectric performance of nanostructured CNTs/ $\text{BiSbTe}$  bulk composite from rapid pressure-quenching induced multi-scale microstructure, *J. Materiomics*, 2016, **2**, 316–323.
- 84 Y. Zhang, H. Ma, B. Sun, B. Liu, H. Liu, L. Kong, B. Liu, X. Jia and X. Chen, Thermoelectric performance of graphene composited  $\text{BiSbTe}$  bulks by high pressure synthesis, *J. Alloys Compd.*, 2017, **715**, 344–348.
- 85 B. Liu, H. Ma, Q. Chen, Y. Wang, G. Ji, X. Li, Y. Zhang and X. Jia, Optimization and modulation for the moderate and high temperature thermoelectric properties of  $\text{PbSe}$  via solid solution with  $\text{PbS}$  synthesized by HPHT, *Mod. Phys. Lett. B*, 2020, 2050185.
- 86 L. Deng, J. Ni, J. Qin and X. Jia, High pressure synthesis and thermoelectric properties of micro/nano structures  $\text{CoSb}_3$ , *J. Solid State Chem.*, 2017, **255**, 129–132.
- 87 L. Wang, L. Deng, J. Qin and X. Jia, Enhanced Thermoelectric Properties of Double-Filled  $\text{CoSb}_3$  via High-Pressure Regulating, *Inorg. Chem.*, 2018, **57**, 6762–6766.
- 88 L. Wang, J. Ni, X. Jia, J. Qin, X. Guo and L. Deng, The thermoelectric properties of  $\text{Ba}_x\text{In}_{0.2-x}\text{Co}_4\text{Sb}_{11.5}\text{Te}_{0.5}$  synthesized at different pressure, *J. Alloys Compd.*, 2017, **691**, 452–456.
- 89 L. Deng, J. Ni, L. Wang, X. Jia, J. Qin and B. Liu, Structure and thermoelectric properties of  $\text{In}_x\text{Ba}_y\text{Co}_4\text{Sb}_{12}$  samples prepared by HPHT, *J. Alloys Compd.*, 2017, **712**, 477–481.
- 90 L. Deng, L. Wang, J. Ni, J. Qin, X. Jia and H. Ma, Enhanced thermoelectric properties of Te-doped and In, Ba double-filled  $\text{CoSb}_3$  composites by high pressure technology, *Mater. Lett.*, 2018, **217**, 44–47.
- 91 L. Deng, J. Qin, X. Jia and X. Guo, Enhanced thermoelectric performance of skutterudites via orthogonal experimental design, *J. Alloys Compd.*, 2017, **695**, 3152–3155.
- 92 J. Chen, X. Jia, Y. Zhang, H. Liu, B. Liu, J. Wang, L. Ding, G. Ji and H. Ma, N-type  $\text{Ba}_{0.2}\text{Co}_4\text{Sb}_{11.5}\text{Te}_{0.5}$ : Optimization of thermoelectric properties by different pressures, *Mod. Phys. Lett. B*, 2019, **33**, 1950027.
- 93 L. Deng, J. Ni, J. Qin and X. Jia, Enhancement of thermoelectric properties of In-filled and Te-doped  $\text{CoSb}_3$  synthesized by high pressure technique, *Mater. Lett.*, 2017, **205**, 110–113.
- 94 L. Deng, D.-N. Li, J.-M. Qin and Q. Duan, Effect of Pb Filling and Synthesis Pressure Regulation on the Thermoelectric Properties of  $\text{CoSb}_3$ , *Inorg. Chem.*, 2019, **58**, 4033–4037.
- 95 H. Sun, X. Jia, L. Deng, P. Lv, X. Guo, Y. Zhang, B. Sun, B. Liu and H. Ma, Effect of HPHT processing on the structure, and thermoelectric properties of  $\text{Co}_4\text{Sb}_{12}$  co-doped with Te and Sn, *J. Mater. Chem. A*, 2015, **3**, 4637–4641.
- 96 H. Sun, P. Lv, C. Wang, Y. Liu, X. Jia and H. Ma, HPHT synthesis and enhanced TE performance of Te and Sn/Se elements binary-doped  $\text{CoSb}_3$ , *Funct. Mater. Lett.*, 2019, **12**, 1850105.
- 97 Y. Jiang, X. Jia and H. Ma, The thermoelectric properties of  $\text{CoSb}_3$  compound doped with Te and Sn synthesized at different pressure, *Mod. Phys. Lett. B*, 2017, **31**, 1750261.
- 98 J. Li, X. Li, C. Chen, W. Hu, F. Yu, Z. Zhao, L. Zhang, D. Yu, Y. Tian and B. Xu, Enhanced thermoelectric performance of bismuth-doped magnesium silicide synthesized under high pressure, *J. Mater. Sci.: Mater. Electron.*, 2018, **53**, 9091–9098.
- 99 J. Li, X. Li, B. Cai, C. Chen, Q. Zhang, Z. Zhao, L. Zhang, F. Yu, D. Yu and Y. Tian, Enhanced thermoelectric performance of high pressure synthesized Sb-doped  $\text{Mg}_2\text{Si}$ , *J. Alloys Compd.*, 2018, **741**, 1148–1152.
- 100 J. Wei, B. Duan, J. Li, H. Yang, G. Chen and P. Zhai, High pressure synthesis of multiple doped  $\text{Mg}_2\text{Si}$ -based thermoelectric materials, *J. Mater. Sci.: Mater. Electron.*, 2018, **29**, 10904–10910.
- 101 L. Zhang, Y. Wang, J. Lv and Y. Ma, Materials discovery at high pressures, *Nat. Rev. Mater.*, 2017, **2**, 17005.
- 102 J. Li, L. Sun, X. Wang, H. Zhu and M. Miao, Simple Route to Metal cyclo- $\text{N}_5$ -Salt: High-Pressure Synthesis of  $\text{CuN}_5$ , *J. Phys. Chem. C*, 2018, **122**, 22339–22344.
- 103 D. Laniel, G. Weck, G. Gaiffe, G. Garbarino and P. Loubeyre, High-pressure synthesized lithium pentazole compound metastable under ambient conditions, *J. Phys. Chem. Lett.*, 2018, **9**, 1600–1604.
- 104 W. Wang, H. Wang, Y. Liu, D. Li, F. Tian, D. Duan, H. Yu and T. Cui, High-Pressure Bonding Mechanism of Selenium Nitrides, *Inorg. Chem.*, 2019, **58**, 2397–2402.
- 105 J. Li, K. Wang, S. Song, X. Qi, W. Zhang, M. Deng and Q. Zhang,  $[\text{LiNa}(\text{N}_5)_2(\text{H}_2\text{O})_4] \cdot \text{H}_2\text{O}$ : a novel heterometal-



- lic cyclo-N<sub>5</sub>– framework with helical chains, *Sci. China Mater.*, 2019, **62**, 283–288.
- 106 Y. Xu, P. Wang, Q. Lin and M. Lu, A carbon-free inorganic–metal complex consisting of an all-nitrogen pentazole anion, a Zn(II) cation and H<sub>2</sub>O, *Dalton Trans.*, 2017, **46**, 14088–14093.
  - 107 Y. Xu, Q. Wang, C. Shen, Q. Lin, P. Wang and M. Lu, A series of energetic metal pentazolate hydrates, *Nature*, 2017, **549**, 78–81.
  - 108 X. Shi, Z. Yao and B. Liu, New High Pressure Phases of the Zn–N System, *J. Phys. Chem. C*, 2020, **124**, 4044–4049.
  - 109 S. Wei, L. Lian, Y. Liu, D. Li, Z. Liu and T. Cui, Pressure-Stabilized Polymerization of Nitrogen in Alkaline-Earth-Metal Scandium Nitrides, *Phys. Chem. Chem. Phys.*, 2020, **22**, 5242–5248.
  - 110 Q. Li, L. Sha, C. Zhu and Y. Yao, New multifunctional tungsten nitride with energetic N<sub>6</sub> and extreme hardness predicted from first principles, *EPL*, 2017, **118**, 46001.
  - 111 G. Ackland, High-pressure phases of group IV and III–V semiconductors, *Rep. Prog. Phys.*, 2001, **64**, 483–516.
  - 112 F. M. Shakhov, A. M. Abyzov and K. Takai, Boron doped diamond synthesized from detonation nanodiamond in a COH fluid at high pressure and high temperature, *J. Solid State Chem.*, 2017, **256**, 72–92.
  - 113 Y. Li, S. Li, M. Song, Y. She, Q. Wang and X. Guan, Synthesis of n-type semiconductor diamond single crystal under high pressure and high temperature, *IOP Conf. Ser.: Mater. Sci. Eng.*, 2017, **274**, 012131.
  - 114 C. Gong, S. Li, H. Zhang, T. Su, M. Hu, H. Ma, X. Jia and Y. Li, Study on synthesis and electrical properties of slab shape diamond crystals in FeNiMnCo–CP system under HPHT, *Int. J. Refract. Met. Hard Mater.*, 2017, **66**, 116–121.
  - 115 X. Liu, X. Chen, D. J. Singh, R. A. Stern, J. Wu, S. Petitgirard, C. R. Bina and S. D. Jacobsen, Boron-oxygen complex yields n-type surface layer in semiconducting diamond, *Proc. Natl. Acad. Sci. U. S. A.*, 2019, **116**, 7703–7711.
  - 116 Y. Hinuma, T. Hatakeyama, Y. Kumagai, L. A. Burton, H. Sato, Y. Muraba, S. Iimura, H. Hiramatsu, I. Tanaka and H. Hosono, Discovery of earth-abundant nitride semiconductors by computational screening and high-pressure synthesis, *Nat. Commun.*, 2016, **7**, 11962.
  - 117 N. Solopova, N. Dubrovinskaia and L. Dubrovinsky, Synthesis of nanocrystalline diamond from glassy carbon balls, *J. Cryst. Growth*, 2015, **412**, 54–59.
  - 118 M. Terasawa, S.-i. Honda, K. Niwase, M. Niibe, T. Hisakuni, T. Iwata, Y. Higo, T. Shinmei, H. Ohfuji and T. Irifune, Nano-polycrystalline diamond synthesized from neutron-irradiated highly oriented pyrolytic graphite (HOPG), *Diamond Relat. Mater.*, 2018, **82**, 132–136.
  - 119 M. J. Crane, B. E. Smith, P. B. Meisenheimer, X. Zhou, R. M. Stroud, E. J. Davis and P. J. Pauzauskie, Photothermal effects during nanodiamond synthesis from a carbon aerogel in a laser-heated diamond anvil cell, *Diamond Relat. Mater.*, 2018, **87**, 134–142.
  - 120 M. J. Crane, A. Petrone, R. A. Beck, M. B. Lim, X. Zhou, X. Li, R. M. Stroud and P. J. Pauzauskie, High-pressure, high-temperature molecular doping of nanodiamond, *Sci. Adv.*, 2019, **5**, eaau6073.
  - 121 E. Ekimov, S. Lyapin, Y. V. Grigoriev, I. Zibrov and K. Kondrina, Size-controllable synthesis of ultrasmall diamonds from halogenated adamantanes at high static pressure, *Carbon*, 2019, **150**, 436–438.
  - 122 E. Ekimov, M. Kondrin, V. Krivobok, A. Khomich, I. Vlasov, R. Khmelnitskiy, T. Iwasaki and M. Hatano, Effect of Si, Ge and Sn dopant elements on structure and photoluminescence of nano- and microdiamonds synthesized from organic compounds, *Diamond Relat. Mater.*, 2019, **93**, 75–83.
  - 123 N. Chen, G. Zhang, R. Li, G. Xu, F. Wang, H. Ma and X. Jia, Defect and Stress Reduction in High-Pressure and High-Temperature Synthetic Diamonds Using Gradient Cooling Technology, *Cryst. Growth Des.*, 2020, **20**, 3358–3364.
  - 124 W. Hu, B. Wen, Q. Huang, J. Xiao, D. Yu, Y. Wang, Z. Zhao, J. He, Z. Liu and B. Xu, Role of plastic deformation in tailoring ultrafine microstructure in nanotwinned diamond for enhanced hardness, *Sci. China Mater.*, 2017, **60**, 178–185.
  - 125 H. Tang, X. Yuan, P. Yu, Q. Hu, M. Wang, Y. Yao, L. Wu, Q. Zou, Y. Ke and Y. Zhao, Revealing the formation mechanism of ultrahard nanotwinned diamond from onion carbon, *Carbon*, 2018, **129**, 159–167.
  - 126 Q. Tao, X. Wei, M. Lian, H. Wang, X. Wang, S. Dong, T. Cui and P. Zhu, Nanotwinned diamond synthesized from multicore carbon onion, *Carbon*, 2017, **120**, 405–410.
  - 127 H. Tang, M. Wang, D. He, Q. Zou, Y. Ke and Y. Zhao, Synthesis of nano-polycrystalline diamond in proximity to industrial conditions, *Carbon*, 2016, **108**, 1–6.
  - 128 H. Xie, F. Yin, T. Yu, J.-T. Wang and C. Liang, Mechanism for direct graphite-to-diamond phase transition, *Sci. Rep.*, 2014, **4**, 5930.
  - 129 V. Y. Osipov, F. Shakhov, N. Efimov, V. Minin, S. Kidalov and A. Y. Vul, Identification of paramagnetic nitrogen centers (P1) in diamond crystallites synthesized via the sintering of detonation nanodiamonds at high pressure and temperature, *Phys. Solid State*, 2017, **59**, 1146–1153.
  - 130 Y. N. Palyanov, I. N. Kupriyanov, Y. M. Borzdov and N. V. Surovtsev, Germanium: a new catalyst for diamond synthesis and a new optically active impurity in diamond, *Sci. Rep.*, 2015, **5**, 14789.
  - 131 Y. Palyanov, I. Kupriyanov, Y. Borzdov, D. Nechaev and Y. Bataleva, HPHT diamond crystallization in the Mg–Si–C system: effect of Mg/Si composition, *Crystals*, 2017, **7**, 119.
  - 132 S. Sun, Z. Xu, W. Cui, J. Lv, Y. Geng, H. Li, X. Jia and H.-a. Ma, The study on the diamond growth and morphology from light elements (NBH) synergistic doping systems under HPHT, *Int. J. Refract. Met. Hard Mater.*, 2018, **70**, 169–175.
  - 133 Y. N. Palyanov, I. N. Kupriyanov, Y. M. Borzdov, A. F. Khokhryakov and N. V. Surovtsev, High-pressure syn-

- thesis and characterization of Ge-doped single crystal diamond, *Cryst. Growth Des.*, 2016, **16**, 3510–3518.
- 134 H. Zhang, S. Li, G. Li, T. Su, M. Hu, H. Ma, X. Jia and Y. Li, Effect of BS co-doping on large diamonds synthesis under high pressure and high temperature, *Int. J. Refract. Met. Hard Mater.*, 2017, **66**, 26–30.
  - 135 X. Miao, L. Chen, H. Ma, C. Fang, L. Guo, S. Fang, Y. Wang and X. Jia, Studies on HPHT synthesis and N defects of N-rich B-doped diamonds, *CrystEngComm*, 2018, **20**, 7109–7113.
  - 136 S. Sun, W. Cui, X. Jia, H.-a. Ma and J. Lv, The synthesis of “BCN” diamond materials with different B/N additives under high pressure and high temperature, *Int. J. Refract. Met. Hard Mater.*, 2016, **59**, 56–60.
  - 137 M. Wang, J. Binns, M.-E. Donnelly, M. Peña-Alvarez, P. Dalladay-Simpson and R. T. Howie, High pressure synthesis and stability of cobalt hydrides, *J. Chem. Phys.*, 2018, **148**, 144310.
  - 138 M. Kutzschbach, B. Wunder, M. Krstulovic, A. Ertl, R. Trumbull, A. Rocholl and G. Giester, First high-pressure synthesis of rossmanitic tourmaline and evidence for the incorporation of Li at the X site, *Phys. Chem. Miner.*, 2017, **44**, 353–363.
  - 139 A. N. Arpita Aparajita, N. R. Sanjay Kumar, S. Chandra, S. Amirthapandian, N. V. C. Shekar and K. Sridhar, High-Pressure Synthesis of Manganese Monocarbide: A Potential Superhard Material, *Inorg. Chem.*, 2018, **57**, 14178–14185.
  - 140 M. Santoro, D. Scelta, K. Dziubek, M. Ceppatelli, F. A. Gorelli, R. Bini, G. Garbarino, J.-M. Thibaud, F. Di Renzo and O. Cambon, Synthesis of 1D polymer/zeolite nanocomposites under high pressure, *Chem. Mater.*, 2016, **28**, 4065–4071.
  - 141 E. Solana-Madruga, A. Dos santos-García, A. Arévalo-López, D. Ávila-Brandé, C. Ritter, J. Attfield and R. Sáez-Puche, High pressure synthesis of polar and non-polar cation-ordered polymorphs of  $\text{Mn}_2\text{ScSbO}_6$ , *Dalton Trans.*, 2015, **44**, 20441–20448.
  - 142 Y. S. Glazkova, N. Terada, Y. Matsushita, Y. Katsuya, M. Tanaka, A. V. Sobolev, I. A. Presniakov and A. A. Belik, High-pressure synthesis, crystal structures, and properties of  $\text{CdMn}_7\text{O}_{12}$  and  $\text{SrMn}_7\text{O}_{12}$  perovskites, *Inorg. Chem.*, 2015, **54**, 9081–9091.
  - 143 Y. Li, J. Cheng, J. A. Alonso, J. B. Goodenough and J. Zhou, High-Pressure Synthesis, Crystal Structure, and Magnetic and Transport Properties of a Six-Layered  $\text{SrRhO}_3$ , *Inorg. Chem.*, 2017, **56**, 8187–8194.
  - 144 L. Ding, D. D. Khalyavin, P. Manuel, J. Blake, F. Orlandi, W. Yi and A. A. Belik, Colossal magnetoresistance in the insulating ferromagnetic double perovskites  $\text{Ti}_2\text{NiMnO}_6$ : A neutron diffraction study, *Acta Mater.*, 2019, **173**, 20–26.
  - 145 W.-D. Wang, A. Li, G.-H. Xu, P. Wang, Y.-G. Liu and L.-P. Wang, Synthesis of Polycrystalline Diamond Compact with Selenium: Discovery of a New Se-C Compound, *Chin. Phys. Lett.*, 2020, **37**, 058101.
  - 146 M. Santoro, K. Dziubek, D. Scelta, M. Ceppatelli, F. A. Gorelli, R. Bini, J.-M. Thibaud, F. Di Renzo, O. Cambon and J. Rouquette, High Pressure Synthesis of All-Transoid Polycarbonyl  $[-(\text{C}=\text{O})-]_n$  in a Zeolite, *Chem. Mater.*, 2015, **27**, 6486–6489.
  - 147 D. Mori, K. Tanaka, H. Saitoh, T. Kikegawa and Y. Inaguma, Synthesis, direct formation under high pressure, structure, and electronic properties of  $\text{LiNbO}_3$ -type oxide  $\text{PbZnO}_3$ , *Inorg. Chem.*, 2015, **54**, 11405–11410.
  - 148 N. S. Kumar, S. Chandra, S. Amirthapandian, N. C. Shekar and P. C. Sahu, Investigations of the high pressure synthesized osmium carbide by experimental and computational techniques, *Mater. Res. Express*, 2015, **2**, 016503.
  - 149 W. Xing, Z. Wei, R. Yu and F. Meng, Prediction of stable high-pressure structures of tantalum nitride  $\text{TaN}_2$ , *J. Mater. Sci. Technol.*, 2019, **35**, 2297–2304.
  - 150 K. H. Hong, E. Solana-Madruga, M. Coduri and J. P. Attfield, Complex Cation and Spin Orders in the High-Pressure Ferrite  $\text{CoFe}_3\text{O}_5$ , *Inorg. Chem.*, 2018, **57**, 14347–14352.
  - 151 P. Yu, L. Zhang, H. Tang, J. Fan, P. K. Liaw, G. Li and R. Liu, Formation, reverse transformation, and properties of  $\epsilon$ -martensite phase in the  $\text{CoCrFeMnNi}$  high-entropy alloy under high-pressure, *J. Alloys Compd.*, 2019, **779**, 1–6.
  - 152 C. L. Tracy, S. Park, D. R. Rittman, S. J. Zinkle, H. Bei, M. Lang, R. C. Ewing and W. L. Mao, High pressure synthesis of a hexagonal close-packed phase of the high-entropy alloy  $\text{CrMnFeCoNi}$ , *Nat. Commun.*, 2017, **8**, 15634.
  - 153 X.-H. Shi, B. Liu, Z. Yao and B.-B. Liu, Pressure-Stabilized New Phase of  $\text{CaN}_4$ , *Chin. Phys. Lett.*, 2020, **37**, 047101.
  - 154 X. Dong, L. Wang, K. Li, H. Zheng, Y. Wang, Y. Meng, H. Shu, H.-k. Mao, S. Feng and C. Jin, Tailored Synthesis of the Narrowest Zigzag Graphene Nanoribbon Structure by Compressing the Lithium Acetylide under High Temperature, *J. Phys. Chem. C*, 2018, **122**, 20506–20512.
  - 155 M. Bykov, S. Chariton, H. Fei, T. Fedotenko, G. Aprilis, A. V. Ponomareva, F. Tasnádi, I. A. Abrikosov, B. Merle and P. Feldner, High-pressure synthesis of ultraincompressible hard rhenium nitride pernitride  $\text{Re}_2(\text{N}_2)(\text{N})_2$  stable at ambient conditions, *Nat. Commun.*, 2019, **10**, 1–8.
  - 156 V. S. Bhadram, D. Y. Kim and T. A. Strobel, High-pressure synthesis and characterization of incompressible titanium pernitride, *Chem. Mater.*, 2016, **28**, 1616–1620.
  - 157 S. Khandarkhaeva, T. Fedotenko, M. Bykov, E. Bykova, S. Chariton, P. Sedmak, K. Glazyrin, V. Prakapenka, N. Dubrovinskaia and L. Dubrovinsky, Novel rhenium carbides at 200 GPa, 2020, arXiv preprint arXiv:01221.
  - 158 A. Dewaele, N. Worth, C. J. Pickard, R. J. Needs, S. Pascarelli, O. Mathon, M. Mezouar and T. Irifune, Synthesis and stability of xenon oxides  $\text{Xe}_2\text{O}_5$  and  $\text{Xe}_3\text{O}_2$  under pressure, *Nat. Chem.*, 2016, **8**, 784.
  - 159 D. Laniel, A. s. Dewaele and G. Garbarino, High pressure and high temperature synthesis of the iron pernitride  $\text{FeN}_2$ , *Inorg. Chem.*, 2018, **57**, 6245–6251.

- 160 M. Bykov, E. Bykova, G. Aprilis, K. Glazyrin, E. Koemets, I. Chuvashova, I. Kупenko, C. McCammon, M. Mezouar and V. Prakapenka, Fe-N system at high pressure reveals a compound featuring polymeric nitrogen chains, *Nat. Commun.*, 2018, **9**, 1–8.
- 161 M. Bykov, E. Bykova, E. Koemets, T. Fedotenko, G. Aprilis, K. Glazyrin, H. P. Liermann, A. V. Ponomareva, J. Tidholm and F. Tasnádi, High-Pressure Synthesis of a Nitrogen-Rich Inclusion Compound  $\text{ReN}_8 \cdot x\text{N}_2$  with Conjugated Polymeric Nitrogen Chains, *Angew. Chem., Int. Ed.*, 2018, **57**, 9048–9053.
- 162 E. Bykova, H. Gou, M. Bykov, M. Hanfland, L. Dubrovinsky and N. Dubrovinskaia, Crystal structures and compressibility of novel iron borides  $\text{Fe}_2\text{B}_7$  and  $\text{Fe}_x\text{B}_{50}$  synthesized at high pressure and high temperature, *J. Solid State Chem.*, 2015, **230**, 102–109.
- 163 N. N. Patel, A. K. Verma, A. Mishra, M. Sunder and S. M. Sharma, The synthesis of unconventional stoichiometric compounds in the K–Br system at high pressures, *Phys. Chem. Chem. Phys.*, 2017, **19**, 7996–8007.
- 164 K. Powderly, S. Clarke, M. Amsler, C. Wolverton, C. D. Malliakas, Y. Meng, S. D. Jacobsen and D. E. Freedman, High-pressure discovery of  $\beta\text{-NiBi}$ , *Chem. Commun.*, 2017, **53**, 11241–11244.
- 165 M. Akhtar, M. Menon, M. Sunkara, G. Sumanasekera, A. Durygin and J. B. Jasinski, High-pressure synthesis of rhombohedral  $\alpha\text{-AgGaO}_2$  via direct solid state reaction, *J. Alloys Compd.*, 2015, **641**, 87–92.
- 166 F. O. Von Rohr, H. Ji, F. A. Cevallos, T. Gao, N. P. Ong and R. J. Cava, High-Pressure Synthesis and Characterization of  $\beta\text{-GeSe}$ —A Six-Membered-Ring Semiconductor in an Uncommon Boat Conformation, *J. Am. Chem. Soc.*, 2017, **139**, 2771–2777.
- 167 O. O. Kurakevych, Y. Le Godec, W. A. Crichton, J. Guignard, T. A. Strobel, H. Zhang, H. Liu, C. C. Diogo, A. Polian, N. Menguy, S. J. Juhl and C. Gervais, Synthesis of Bulk BC8 Silicon Allotrope by Direct Transformation and Reduced-Pressure Chemical Pathways, *Inorg. Chem.*, 2016, **55**, 8943–8950.
- 168 M. Matsushita, R. Inugai, M. Yamasaki, T. Shinmei, Y. Kawamura, T. Irifune, N. Fujita and E. Abe, A long-period superlattice phase in  $\text{Mg}_{97}\text{Zn}_1\text{Yb}_2$  alloys synthesized under high-pressure, *Scr. Mater.*, 2016, **121**, 45–49.
- 169 I. Kупenko, G. Aprilis, D. Vasiukov, C. McCammon, S. Chariton, V. Cerantola, I. Kantor, A. Chumakov, R. Rüffer and L. Dubrovinsky, Magnetism in cold subducting slabs at mantle transition zone depths, *Nature*, 2019, **570**, 102–106.